

Quantifying water cover shifts across the globe: following the steps of walking floods

Paula Torre Zaffaroni¹, Javier Houspanossian², Carlos M Di Bella¹, and Esteban Gabriel Jobbagy²

¹Instituto de Investigaciones Fisiológicas y Ecológicas Vinculadas a la Agricultura

²IMASL - Universidad Nacional de San Luis/CONICET

July 23, 2023

Abstract

Floods in ideal landscapes follow a coherent pattern where single water-covered areas expand and afterwards recede following the inverse sequence but deviate in real landscapes, due to natural or human factors, resulting in flood coverage shifts. Using remote sensing, we introduced two indices to describe the discrepancies between spatially integrated vs. pixel-level frequency distributions under maximum flooded conditions (dext) and throughout all flooding conditions (dtot), expressed as the relative weight of shifts on each landscape's maximum registered coverage, theoretically ranging between no displacement ($<20\%$) to maximum displacement ($< < \text{inf}$). Globally, over 36 years floods 26 exhibited redistributions representing, on average, 25% and 45% of their peak extents 27 revealing previously unnoticed extra flooded areas and rotational movements within flood28 ing events, rising up to 500% in meandering rivers (South America) and irrigated crop29 lands (Central Asia). We also assessed the influence of natural and human variables and 30 discussed the indices' potential for advancing flood research.

1 **Quantifying water cover shifts across the globe:**
2 **following the steps of walking floods**

3 **P. Torre Zaffaroni^{1,2,3}, J. Houspanossian³, C.M. Di Bella^{1,2}, E.G. Jobbágy³**

4 ¹Instituto de Investigaciones Fisiológicas y Ecológicas Vinculadas a la Agricultura (IFEVA), Facultad de
5 Agronomía, Universidad de Buenos Aires, CONICET, Buenos Aires, Argentina

6 ²Departamento de Métodos Cuantitativos y Sistemas de Información, Facultad de Agronomía,
7 Universidad de Buenos Aires

8 ³Grupo de Estudios Ambientales – IMASL, Universidad Nacional de San Luis & CONICET, San Luis,
9 Argentina

10 **Key Points:**

- 11 • We developed two complementary indices to describe water cover shifts between
12 and within flooding events
13 • Over the last 36 years, shifts expanded the global flooded-affected area by 25%
14 with another 20% redistributing at intermediate stages
15 • Flat topographies, arid climates, and irrigation favor this phenomenon while river
16 dams and channels inhibit it over time

Abstract

Floods in ideal landscapes follow a coherent pattern where single water-covered areas expand and afterwards recede following the inverse sequence but deviate in real landscapes, due to natural or human factors, resulting in flood coverage shifts. Using remote sensing, we introduced two indices to describe the discrepancies between spatially integrated vs. pixel-level frequency distributions under maximum flooded conditions (dext) and throughout all flooding conditions (dtot), expressed as the relative weight of shifts on each landscape's maximum registered coverage, theoretically ranging between no displacement (<20%) to maximum displacement (<< inf). Globally, over 36 years floods exhibited redistributions representing, on average, 25% and 45% of their peak extents revealing previously unnoticed extra flooded areas and rotational movements within flooding events, rising up to 500% in meandering rivers (South America) and irrigated croplands (Central Asia). We also assessed the influence of natural and human variables and discussed the indices' potential for advancing flood research.

Plain Language Summary

While in ideal landscapes flood events should display the same spatial distribution in their expansion and recession stages of any flooding event, real flooding may drift away from this expected pattern. We developed two indices based on remote sensing data to locate where these shifts are important and understand how they are influenced by nature and humans. By analyzing data from around the world, we discovered that thanks to the displacement from the ideal distributions, floods covered globally an extra quarter of the area. Natural factors like low terrain ruggedness and high aridity foster much larger flooding displacement. In regions hosting rivers that carry large quantities of sediment and often change their course (e.g., India and Perú), displacement engages five times more area in floods than ideally expected. We also found that water infrastructure like reservoirs and irrigation also influenced flooding displacement. For instance, displacement was very relevant in intensely irrigated regions like Central Asia and Australia, reflecting surface water deviation as needed for crop production. Because these variations scope flooding spatiotemporal dynamics with important implications for the provision of many ecosystem services, their quantification and assessment allow us to monitor and understand our ongoing imprint on regional flooding dynamics.

1 Introduction

The spatial dynamics of floods, and specifically the pattern of their expansion and recession over the territory, is an important aspect of flooding variability. The flood pulse concept describes a model of flooding where water increasingly covers adjacent areas of already flooded surfaces, and afterward recedes following the exact inverse sequence, along what is described as an aquatic-terrestrial transition zone (Junk et al., 1989; Wantzen et al., 2008, for a definition extended to lentic systems). This null model of fully coherent flood expansion/recession implies that the exact locations that are covered by water can be known for any level of flooding (i.e., any given fraction of water coverage) based on the distribution of previous floods. However, in real landscapes like those occupied by highly meandering rivers, floods do not always proceed in this predictable way, changing locations throughout successive events or by following asymmetrical expansion vs. recession trajectories (Tockner et al., 2000; Finotello et al., 2020). Though it could give important insights into ecosystem functioning at multiple levels, this attribute of flooding dynamics (hereafter, flooding displacement) has not yet been systematically quantified, and has been seldom described in the case of shallow lakes. Instead, flooding displacement has been analyzed in riverbanks through numerical modeling (Camporeale et al., 2005), manual and automatized detection of spatial shifts of water-classified pixels (Lin et al., 2020; Langhorst & Pavelsky, 2023), or, more commonly, included as a known

67 attribute in the design of field experiments and observations (Constantine & Dunne, 2008;
68 Finotello et al., 2020; Walcker et al., 2021) from which a large body of knowledge on the
69 physical laws guiding displacement has been generated (Wren et al., 2008; Van Dijk et
70 al., 2013).

71 The spatiotemporal nature of this phenomenon suggests that it can be explored
72 through remote sensing. A key advantage is its ability to uniformly study one attribute
73 with low costs. With the development of global water masks from the Landsat satellite
74 archive (Pekel et al., 2016a) and cloud processing servers (Gorelick et al., 2017), it is pos-
75 sible to analyze flooding displacement globally for more than three decades. Such infor-
76 mation has already helped to explore the temporal dynamics of floods, including long-
77 term trends (Pekel et al., 2016a; Olthof & Rainville, 2022) and other components of tem-
78 poral variability (Pickens et al., 2020, Torre Zaffaroni et al., in review, submitted to Wa-
79 ter Resources Research, 2023), and even colorimetric characterizations as a proxy of wa-
80 ter quality (Gardner et al., 2021). Moreover, Langhorst and Pavelsky (2023) have shown
81 that the displacement of riverbeds can be assessed through remote sensing, quantifying
82 the direction of erosion and accretion for water courses wider than 100m with excellent
83 results. These studies showcase how optical remote sensing tools can detect detailed as-
84 pects of flooding, presenting an opportunity for comprehensive global characterizations
85 and studies of geographical drivers, despite their limitations such as data gaps caused
86 by cloud coverage and lower resolution for older satellite missions.

87 While climate, topography, and water infrastructure have been pointed out as drivers
88 of flooding displacement, their relative importance in dictating how floods drift away from
89 a coherent regime remains unquantified. In the case of dry regions high runoff and pre-
90 cipitation variability translate into spatially heterogeneous flood events (Tooth, 2000;
91 Brunzell, 2010). Rivers in plains with high geomorphological activity can carry, remove,
92 and deposit large amounts of sediment in their banks fostering migration of courses and
93 the formation of oxbow lakes which retain large masses of water (Richardson et al., 1987;
94 Constantine & Dunne, 2008; Langhorst & Pavelsky, 2023). Because slope, ruggedness,
95 and landforms at a landscape level dictate surface water transport and storage (McGuire
96 et al., 2005; Sivapalan et al., 2011; Rudorff et al., 2014), we hypothesize that topographic
97 characteristics are important determinants of flooding displacement beyond lotic systems.
98 On top of natural drivers, irrigation, particularly in paddy rice cultivation, can contribute
99 to flooding displacement due to varying watering practices in different plots, especially
100 in regions that practice double and triple cropping systems (Sakamoto et al., 2007; Dong
101 et al., 2015). River engineering, such as channelization, canalization, dams, and reser-
102 voirs can minimize flooding displacement by altering river geomorphology and sediment
103 transport downstream (Ward & Stanford, 1995; Vörösmarty et al., 2010; Tena et al., 2020).

104 As flood expansion/recession cycles sustain many ecosystemic functions (Tockner
105 & Stanford, 2002; Pi et al., 2022) including the exchange of greenhouse gases with the
106 atmosphere (Watts et al., 2014; Saunio et al., 2020; Walcker et al., 2021), it is impor-
107 tant to quantify how floods displace over time to better forecast changes in ecosystem
108 function as well as global climate. Remote sensing tools make it feasible to monitor the
109 response of flooding to increasingly variable precipitation regimes (Kundzewicz, 2008;
110 Najibi & Devineni, 2018; Arias et al., 2021), changes in land use and land cover (Twine
111 et al., 2004; Loarie et al., 2011; Kuppel et al., 2015), and mitigation-oriented water man-
112 agement strategies. It can further improve decision-making for flood management and
113 planning by improving the identification of flood-prone areas and their shift across land-
114 scapes.

115 This work addresses the spatial dynamics of floods focusing on flooding displace-
116 ment across events. First, it builds two indices that quantify the degree to which the dis-
117 tribution of floods deviates from a fully coherent expansion/recession pattern (i.e., flood-
118 ing displacement). Second, it maps flood displacement with these indices over the last
119 36 years for the whole globe using remotely sensed data of surface water and evaluates

120 their conjoint performance across gradients of coherence. Finally, it explores how flood-
 121 ing displacement relates to natural and anthropic factors. The ultimate goal is to set the
 122 methodological basis for studying flood displacement patterns and trends using long-term
 123 data of global scope.

124 2 Data and Methods

125 We based our work on high-resolution, remotely sensed data of surface water cov-
 126 erage, using spatially aggregated (single pixels within a grid cell) time series vs. tem-
 127 porally aggregated (single dates across the whole study period) pixel distributions to quan-
 128 tify displacement. The monthly, 30-meter resolution Global Surface Water Extent dataset
 129 (Pekel et al., 2016a) is a powerful tool to analyze regional-level flooding processes, with
 130 available observations going back as far as 1985. Its most recent version (v1.4) extended
 131 the original version up to 2021, inclusive, and can be found in the Google Earth Engine
 132 catalog, the latter which allows the processing of such vast amounts of data.

133 A spatially coherent development of floods should reflect a bucket-like geometry
 134 where, as the flooded area increases, places that were already flooded stay covered by
 135 water, and where one can observe the same distribution of water-covered and water-free
 136 areas for any given fraction of total water coverage in the region in all flood episodes and
 137 regardless of being in the expansion or retraction phase (Figure 1b). In such cases, when
 138 flooded areas are aggregated for a given extent of the territory (e.g., catchment or grid
 139 cell) the overall floodable area (sum of all the individual pixels that were covered by wa-
 140 ter at any point in the time period) should match the maximum flooded extent (sum of
 141 all the pixels that were covered by water when flooding reached its maximum coverage
 142 in the region), and the recession of flooding should mirror its development exactly with
 143 the first drying areas being the last ones that got flooded. Taking this hypothetical sit-
 144 uation as a null model, we measured two aspects through which departures from this pat-
 145 tern can emerge. The accompanying schematization for three alternative hypothetical
 146 situations is found in Figure 1 (c-e). First, we defined the extreme displacement (d_{ext})
 147 as the relative difference between the overall flooded extent (O), which is the sum of all
 148 pixels that were covered by water at any point in time, and the maximum extent observed
 149 simultaneously at any particular month in the spatially-aggregated time series (Mx) (Eq.
 150 1).

$$151 \quad d_{ext} = \frac{O - Mx}{Mx} \quad (1)$$

152 This index represents the fraction of area that escaped some individual peak events
 153 but was still engaged in flooding and is assumed to have been gained from the dry frac-
 154 tion of the landscape. It is easily interpreted as the fraction of the area that missed the
 155 flood at the time of maximum coverage, providing valuable information about the wetting-
 156 drying dynamic of the region. For this reason, it should be more sensitive for analyzing
 157 individual events or dynamics in which different fractions of the landscape engage in each
 158 flood event, more commonly found in irrigated landscapes (Figure 1c).

159 The previous extreme displacement quantification may underestimate flood displace-
 160 ment taking place at intermediate levels of water coverage or highly rotating floods, such
 161 as those experienced in high-intensity irrigated landscapes where the flooding sequence
 162 of plots is erratic (Figure 1d). It could also fall short of capturing flood dynamics where
 163 engaged areas may converge beyond a certain threshold of water coverage but not be-
 164 low it (i.e., yielding $d_{ext} = 0$; Figure 1e), and where still the observed apportionment of
 165 flooding frequency among pixels differs greatly from a coherent pattern. In such cases,
 166 the exceeding area does not result just from the dry fraction of the landscape but also
 167 from what we would expect to be highly flooded areas, producing more temporary wa-

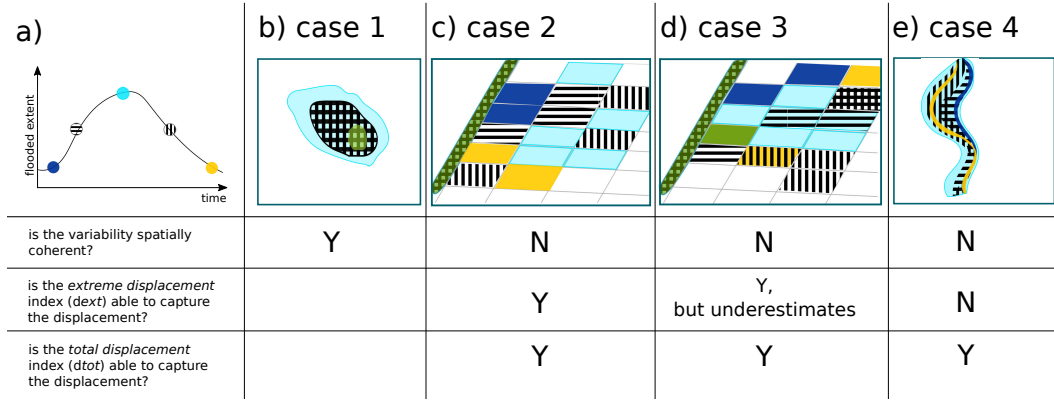


Figure 1. Four alternative hypothetical configurations of flooding for the same temporal series of spatially-aggregated water coverage (a). Cases include: (b) coherent flooding dynamic where the last flooded areas are the first to dry, commonly observed in lakes; (c) incoherent flooding dynamic where each plot is flooded in a rotative way such that each one is covered by water at only one time-step, a situation that could take place in low-to-medium intensity irrigated regions; (d) incoherent flooding dynamic where plots are alternately and variably flooded, a situation expected in high intensity irrigated regions; (e) incoherent flooding dynamic where the spatial pattern of the wetting and drying phase diverges, which can be expected in branched and meandering rivers and their surrounding floodplains as well as hydrologically connected wetlands. Coherence and the ability of the two indices (d_{ext} and d_{tot}) to capture displacement are indicated (yes/no).

168 ter bodies than expected by the information extracted from a spatially aggregated flood
 169 time series.

170 Given the potential underestimation of displacements by the first index presented
 171 above, we constructed a total displacement index (d_{tot}) by comparing two different flooded
 172 area frequency distributions. The first one (temporal distribution, T) results from re-
 173 arranging the time series of monthly surface water extent in a decreasing array. Assum-
 174 ing a null model where the aggregated monthly flood extent accurately represents the
 175 flooding dynamics within the region, this rearrangement would show (1) the maximum
 176 floodable area (i.e., the first observation where all pixels that can be flooded are flooded);
 177 (2) the minimum flooded area or permanent water fraction (i.e., the lowest extent ob-
 178 served, which could also be zero); and (3) the flooding frequency distribution per frac-
 179 tion of area, which is obtained by calculating the difference between observations, start-
 180 ing from the maximum. For example, a region where the maximum observed event across
 181 10 years (i.e., 120 monthly observations) accounted for 1% of the area and the next biggest
 182 event accounted for 0.9% of the area should show 0.1% of its area with a flooding fre-
 183 quency of 1/120 (0.83%). Then, if the null model is representative of the flooding dy-
 184 namics in this region, T reflects the relative contribution of pixels with different individ-
 185 ual flooding frequencies, which can be estimated independently by measuring the dis-
 186 tribution of the actual flooding frequencies, as the percentage of observations with wa-
 187 ter, at the pixel level (30x30 m²) (S). The mismatch between T and S can be quantified
 188 as shown in Eq. 2:

$$189 \quad d_{tot} = \frac{\sum_0^{100} T_n - S_n}{Mx} \quad for T_n > S_n$$

(2)

190

191 where T_n and S_n are the n th frequency flooded area according to the temporal and
192 spatial distributions, respectively. We standardize the mismatches to the maximum sur-
193 face water extent event (Mx) of the region, and thus d_{tot} expresses the equivalent frac-
194 tion of Mx that floods as a result of changing water-covered area locations within and
195 between flooding events.

196 The described phenomenon can be characterized across multiple spatial scales of
197 analyses, comparing upper-level behavior's concordance with their lower-level compo-
198 nents' dynamic (e.g., pixels in remotely sensed data). For this global scope study, we chose
199 a large landscape scale as our focal level, arranging a 1-degree grid ($\sim 111 \times 111$ km at the
200 Equator). After excluding cells that included the ocean surface (12,500 resulting cells),
201 we obtained the landscape-level surface water extent for each cell and month between
202 1985 and 2021, and further filtered (i) time series, keeping observations with over 70%
203 of data available across the cell, and (ii) grid cells, keeping those with over 0.1% of max-
204 imum surface water extent and 30 observations, to reduce noise effects. As a result, we
205 analyzed 10,047 cells over all continents except Antarctica. To illustrate how the displace-
206 ment indices can be applied, we investigated the impact of natural and human factors
207 on flooding location changes within and between events. Boosted regression trees were
208 used to relate flooding displacement with topographical, climatological, hydrological, and
209 agricultural variables (see Supporting Information for more details). The processing of
210 the surface water extent dataset was done in Google Earth Engine, and posterior anal-
211 yses were completed in an R environment (R Core Team, 2021).

3 Results and Discussion

3.1 Flooding displacement characterization

Based on remote sensing data, we developed a novel way to study how floods move across land revealing that their displacement, at varying degrees, is a widespread phenomenon, not only relevant in riverbanks but also important in shallow lakes and irrigated areas worldwide. Both displacement indices developed (d_{ext} and d_{tot}) were able to capture patterns where flooded areas change location throughout events. Through these novel indices, we discovered that close-to-fully coherent flooding patterns (i.e., no displacement) took place in lotic systems including floodplain sections across the Kunene, Ob and Paraguay Rivers in Angola, Russia, and Paraguay, respectively (d_{ext} and $d_{tot} < 0.2$), while in other regions displacement was so large that it exposed to flooding up to five times more area than expected from a coherent pattern such as in the floodplains of the Ucayali and Purús rivers in South America (d_{ext} and $d_{tot} > 1$) known for their high sediment load and dynamic geomorphology. In lotic systems, flooding displacement could result from different expansion patterns associated with the alternance of water source (Tockner et al., 2000), or from hysteretic patterns (i.e. non-symmetrical expansion/recession trajectories) related with riverine geomorphology (Poole, 2010). Yet, this pattern was also extended to lentic systems, for instance those in the northern Undulating Pampas in Argentina composed of very shallow lakes where there is a delicate, water table-mediated flood-generating mechanism (Kuppel et al., 2015). This suggested the usefulness of the indices for discriminating sites in which different flooding mechanisms may prevail (Van Dijk et al., 2013; Wu et al., 2023), and even for comparing their actual development overtime against the simulations of their expected behavior (Camporeale et al., 2005; Rudorff et al., 2014).

Different flooding regimes fostering displacement became evident after comparing the performance of both indices across 10,047, 1°-gridded landscapes (Figure 2). Low values of both d_{ext} and d_{tot} were indicative of coherent patterns where floods expanded and receded following the same geometrical path, such as that in well-defined lake basins (Figure 2a & b). Increases in either index could be attributed to redistribution of flooding between events or within individual events. For instance, greater differences in favor of d_{tot} (Figure 2d-f) suggested shifting patterns with a maximum event that covers all floodable pixels, as a result of intense rainfall, snowmelt, or upstream runoff pulses (as exemplified in Figure 1e). The overlap of maximum and overall extents was almost perfect, yet as much as 40% of the overall floodable extent alternated over time. In certain riverplains (e.g., in sections of the Ob' River, Figure 2d), this behavior had a marginal impact, accounting for less than 20% of water cover shifts. Elsewhere, higher d_{tot} values illustrated the evaporative dynamics of the Eyasi Lake and Aral Sea in Eastern Africa and Central Asia (Figure 2e-f). This type of displacement was more representative of the greatest water-covered landscapes (Figure 2 top-left panel, blue points). Finally, visual interpretation of cells with very high values of d_{ext} and d_{tot} suggested their sensitivity to both natural and human imprints on the distribution of flooded areas (Figure 2g-i).

Flooding displacement indices complement common flooding attributes, highlighting the contribution of this novel approach (Figure S2). Typical indicators of flooding variability include minimum, mean, and maximum extents, and coefficient of variation derived from spatially-aggregated flooded extent time series (e.g., Papa et al., 2008, 2010; Pickens et al., 2020). Our quantitative assessment of flooding redistribution appeared to complement flooding analysis (i.e., were poorly correlated) based upon the aggregation of higher resolution data, independently of their magnitude (i.e., for rarely flooded regions as well as for those hosting floods across the entire landscape), or how temporally variable they were (i.e., from very stable to highly erratic floods). This was suggestive of the value of the indices as, for instance, ephemeral and shallow water bodies fluctuating in size and volume, but also in location -as the indices capture- tend to be

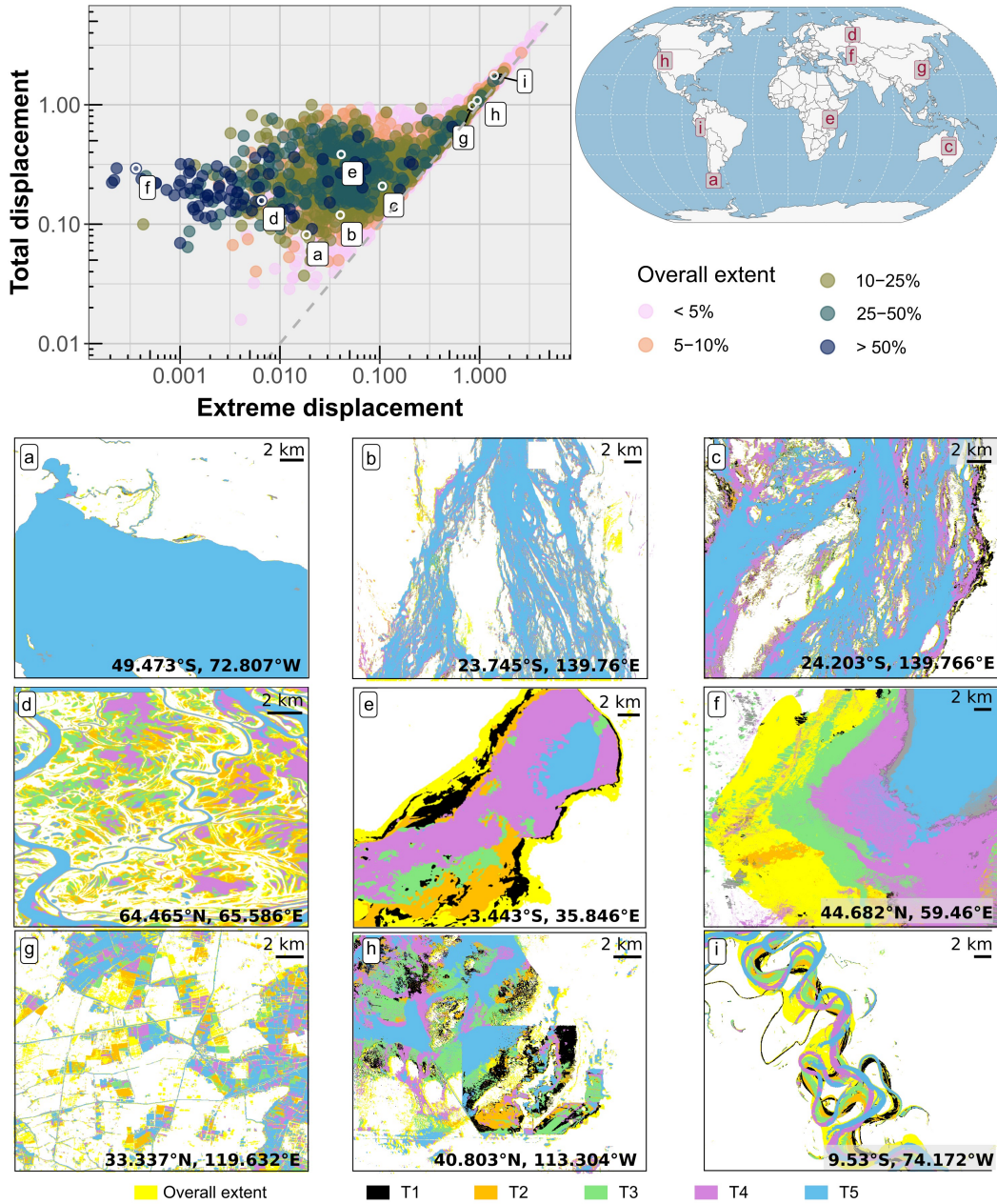


Figure 2. Values assumed for the two proposed flooding displacement indices (extreme displacement, d_{ext} , and total displacement, d_{tot}) across 10,047 1-degree landscapes. Top-right panel: log-log scatter plot coloring cells according to their overall flood extent (i.e., the fraction of area that has been flooded at least once in the last 36 years), with the gray dotted line reflecting the equality line between both indices. (a-i) Examples of the (mis)matches between the overall flooded extent (yellow background) and the geographical contribution of fractions of the landscape in five moments (T1 to T5). (a) Lake Viedma, Argentina; (b-c) Diamantina River, Australia; (d) Ob' River, Russia; (e) Eyasi Lake, Tanzania; (f) Aral Sea, Kazakhstan; (g) Zhenjiang, China (triple cropping hotspot); (h) Salt Flats, United States (partially exploited); (i) Ucayali River, Perú.

265 key contributors to greenhouse gas emissions (Saunio et al., 2020; Walcker et al., 2021),
266 and whose wetting/drying dynamics may have been underestimated with current aggre-
267 gation approaches (Davidson et al., 2018).

268 3.2 Global patterns of flooding displacement

269 Regional clusters of high flooding displacement became evident after mapping the
270 two indices (d_{ext} and d_{tot}) globally (Figure 3). The general similarity between both in-
271 dices suggested that the dominant displacement component is the shift of the water masses
272 across events (e.g. Figure 1c), while erratic rotation (of river channels or irrigated plots,
273 e.g., Figure 1d) has a secondary role and only in a subset of regions. The geographical
274 distribution of flooding displacement showed river valleys in South America and Cen-
275 tral Asia with the greatest degrees of displacement (captured by both indices, e.g., Fig-
276 ure 2g-i), followed by mountainous rivers and irrigation-dense regions further captured
277 by the total displacement index (e.g., Figure 1d-e). The highest displacement took place
278 in the tropics and subtropics including the Bermejo, Ganges, Orinoco, and Ucayali rivers
279 in Argentina, India, Venezuela, and Peru, respectively. All these riverbeds host water
280 courses that reach flat humid plains after leaving young mountain ranges with high sed-
281 iment production (Chakrapani, 2005). Episodes of overflow in meandering and braided
282 rivers that transport high contents of sediments periodically change their main and side
283 courses, likely driving massive flood displacements in these areas (Constantine & Dunne,
284 2008).

285 Besides tropical and subtropical hotspots of displacement fostered by large, and
286 geomorphologically dynamic riverplains, the rest of the world appeared less affected by
287 shifts in the maximum water-covered area, as captured by d_{ext} , with an average of 0.25
288 (i.e., 25% more floodable area than that covered by their highest individual event). Yet,
289 some regions were characterized by patterns in which displacement at intermediate flood-
290 ing levels was more prominent (d_{tot} averaged 0.45) (Figure 2d-f). Examples of this be-
291 havior included the tundra shallow lakes region across the Canadian Shield and an irrigation-
292 dense area along the northern edge of the Tibetan Plateau. Such cases were indicative
293 of flooding patterns where, outside high pulses that covered all floodable areas, there may
294 have been shifts overtime between flood pulses, for instance through the alternation of
295 single, double, and triple rice cropping in rice-intensive regions (Sakamoto et al., 2007;
296 Chen et al., 2012; Tran et al., 2018). The regional imprint of flood irrigation for crop-
297 land production was detected through flooded patches shifting along tropical rivers in
298 Central Asia as well as in other displacement hotspots found in rivers of other parts of
299 central Asia (Yarkand and Aksu), southeastern Australia (Murray), and eastern China
300 (Yellow and Yangtze). These areas match some of the most infrastructure-dense land-
301 scapes as evidenced in literature and through visual interpretation of high-definition im-
302 ages (Siebert et al., 2015; Zeng et al., 2016; Liu, 2022).

303 Remarkably, the lowest displacement (d_{ext} and $d_{tot} < 0.3$) was characteristic of most
304 of the boreal belt, especially across northern North America, Europe, and the vast ma-
305 jority of Russia. Local flooding dynamics were well captured at the landscape level with
306 an approximate concentric expansion and retraction dynamic, possibly explained by the
307 temperature-dominated (as opposed to precipitation-dominated) timing of floods (Papa
308 et al., 2008; Kireeva et al., 2020, Torre Zaffaroni et al., in review, submitted to Water
309 Resources Research, 2023) as well as the glacial processes that have shaped the topog-
310 raphy of these landscapes in the past (i.e., a currently inactive geomorphological agent)
311 that may constrain flooding to well-defined paths water follows (Buttle et al., 2016; Blöschl
312 et al., 2020).

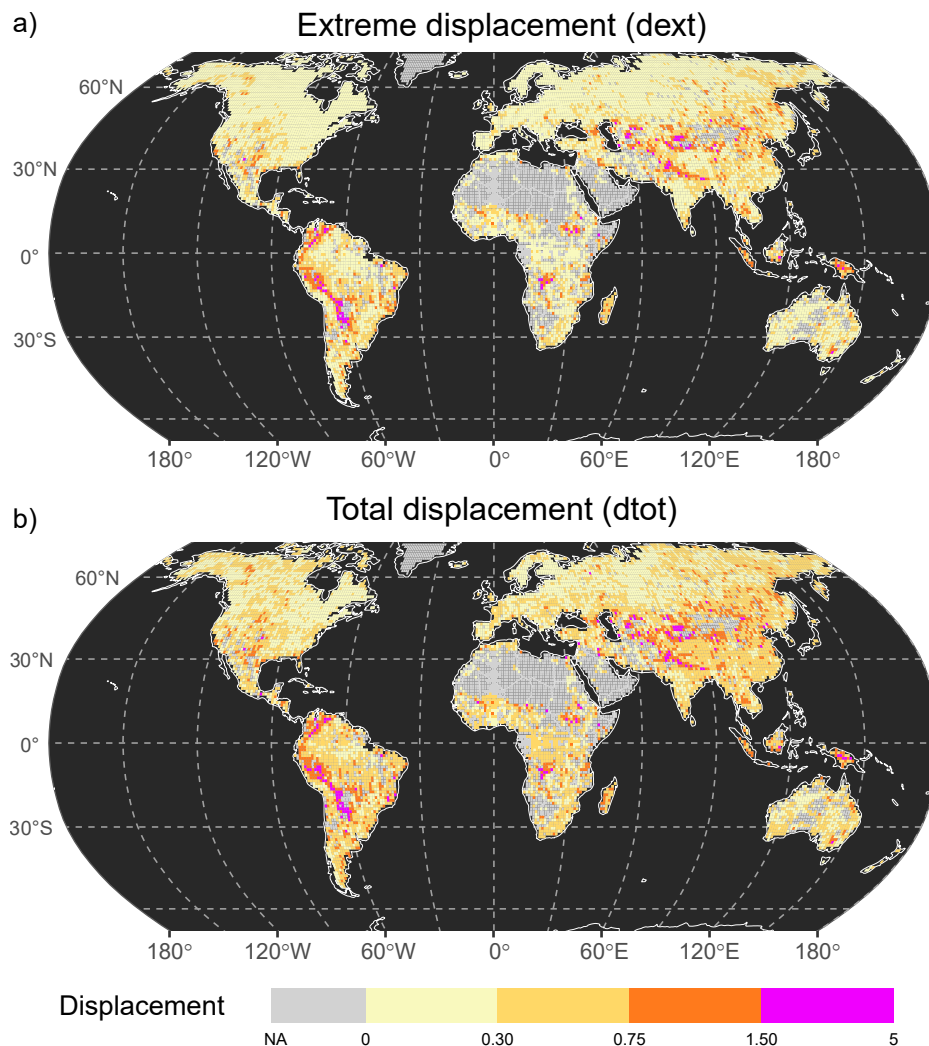


Figure 3. Global distribution of flooding displacement as described by two indices, (a) by obtaining the overall flooded area exceeding the maximum observed flooded area at any particular month (extreme displacement, d_{ext}), (b) by quantifying mismatches between the distribution of flooded frequency pixels and a null model given by the arrangement of landscape-aggregated time series of flooded extent (total displacement, d_{tot}). An interactive online map is available at <https://torrezaffaroni.users.earthengine.app/view/walking-floods>

313

3.3 Natural vs. human drivers of flooding displacement

314

315

316

317

318

319

320

321

Globally, natural drivers were on average more influential on flooding displacement than human drivers related to water management practices as shown by boosted regression trees (Figure S3, see Supplementary Information for more details). Across natural drivers, lake fraction, and local and regional indicators of ruggedness were the most important controls on flooding displacement. Extremely flat regions (regional terrain ruggedness index < 80m), despite pronounced local slopes, foster flooding displacement, aligning with the slower convergence effect observed in the absence of well-defined drainage systems (Figure S4) (McGuire et al., 2005; Aragón et al., 2011). The average distance

322 between meanders, a quantitative indicator of river meandering, ranked fourth in influ-
 323 encing flooding displacement. This corroborated our observation that the indices can de-
 324 tect these highly dynamic landscapes, which provide numerous important ecosystem ser-
 325 vices worldwide (Opperman et al., 2010; Angelini et al., 2013; Walcker et al., 2021). Cli-
 326 mate was strongly related to displacement, with aridity (mean annual precipitation to
 327 potential evapotranspiration ratio < 0.5) favoring it, perhaps as a result of the higher
 328 spatial variability of precipitation events causing floods (Tooth, 2000; Acworth et al., 2016;
 329 Griffin-Nolan et al., 2021).

330 Across human drivers, the density of reservoir and irrigation infrastructure dimin-
 331 ished and enhanced flooding displacement, respectively, with the latter being more in-
 332 fluential even than paddy for rice and rainfed agriculture (Figure S4). Irrigation man-
 333 agement’s impact on this aspect of flooding emphasizes the need to consider its role in
 334 regional hydrology modeling. This can enhance the representation of multiple land and
 335 atmospheric processes, including greenhouse gas emissions and local climate variability
 336 (Loarie et al., 2011; Houspanossian et al., 2018; Saunio et al., 2020). Our findings were
 337 similar for d_{ext} (Figure S5), with lake fraction exerting greater influence than river me-
 338 andering, and floodplain and irrigation coverage, possibly due to the lower capacity of
 339 this index in capturing such displacement patterns (Figure 1d-e).

340 Furthermore, the proposed indices may help in exploring how displacement changes
 341 in a given landscape as it is modified either gradually (e.g., due to increasing irrigation-
 342 allocated areas) or more abruptly (e.g., due to dam emplacements). As an example, we
 343 explored the landscape encompassing two water infrastructure projects in central China
 344 (Three Gorges Dam, built on the Yangtze River between 1994 and 2003, and the Shuibuya
 345 Dam built on the Qingjiang River between 2002 and 2008), revealing a sharp decrease
 346 of flood displacement (d_{ext} from 1.42 to 0.43, Figure S6).

347 4 Conclusions

348 The distribution of floods within a landscape and its variation through time is a
 349 critical but neglected aspect of hydrological analysis and its significance can be overlooked
 350 when examining aggregated flooded areas over time. We tackled this gap by develop-
 351 ing two indices, complementary to those typically employed to assess the temporal at-
 352 tributes of floods, that capture the disparities between the actual spatiotemporal dis-
 353 tribution of flooded areas in a landscape and a null model of spatially coherent flood-
 354 ing in which water-covered areas expand and recede following symmetrical patterns in
 355 each event. Owing to this type of displacement, landscapes worldwide had 45% more area
 356 engaged in flooding episodes between 1985 and 2021 than what their single maximum
 357 flooding levels may have indicated. The highest additions occurred in South American
 358 and Asian landscapes dominated by large meandering rivers transporting sediments from
 359 some of the most tectonically active mountain ranges on Earth to their adjacent plains.
 360 Our results also showed that flat arid and tropical regions experienced the most signif-
 361 icant displacement of flooded areas due to natural and human influences, while boreal
 362 regions had the most spatially coherent flooding events, likely due to their glacially-shaped
 363 landscapes.

364 Water coverage displacement characterization and its uniform application world-
 365 wide with the proposed indices have significant implications for understanding the in-
 366 fluences of flooding on local and global climate as well as for evaluating the distant ef-
 367 fects of land use change, such as deforestation and water infrastructure development, on
 368 hydrological regimes. Our indices demonstrate the potential applications through visual
 369 correspondence and explorative quantitative assessment. We hope to stimulate further
 370 research on this topic and contribute to a more comprehensive understanding of the com-
 371 plex dynamics of flooding in various landscapes. Our study underscores the need for more
 372 integral approaches to flood modeling and management.

5 Open Research

Global flooded extent was derived from JRC’s Global Surface Water dataset v1.4 (Pekel et al., 2016b) available in the Google Earth Engine Data Catalog. Anthromes were downloaded from <https://dataverse.harvard.edu/dataset.xhtml?persistentId=doi:10.7910/DVN/GOQDNQ> (Ellis & Klein Goldewijk, 2019). River segment characterization was extracted from <https://zenodo.org/record/2582500> based on Global River Width from Landsat (Frasson et al., 2019). Global Lakes and Wetlands Database Level 3 (GLWD-3 Lehner & Döll, 2004) was downloaded from <https://www.worldwildlife.org/publications/global-lakes-and-wetlands-database-lakes-and-wetlands-grid-level-3> (Lehner & Döll, 2004). The aridity index was calculated based on TerraClimate long-term averages of annual precipitation-to-potential evapotranspiration ratios (Abatzoglou et al., 2018), while terrain attributes were calculated based on Global Multi-resolution Terrain Dataset (USGS), both available in the Google Earth Engine Data Catalog. The codes for characterizing displacement in Google Earth Engine and analyzing it in R, along with the database, with all variables aggregated to the 1-degree grid, can be found at <https://zenodo.org/record/8083689>.

Acknowledgments

This work was supported by CONICET (PIP 11220200100363CO, PIBBA 28720210100697CO). The authors declare no conflict of interest.

References

- Abatzoglou, J. T., Dobrowski, S. Z., Parks, S. A., & Hegewisch, K. C. (2018). *Terraclimate: Monthly climate and climatic water balance for global terrestrial surfaces, university of idaho* [dataset]. Retrieved from https://developers.google.com/earth-engine/datasets/catalog/IDAHO_EPSCOR_TERRACLIMATE doi: 10.1038/sdata.2017.191
- Acworth, R. I., Rau, G. C., Cuthbert, M. O., Jensen, E., & Leggett, K. (2016). Long-term spatio-temporal precipitation variability in arid-zone Australia and implications for groundwater recharge. *Hydrogeology Journal*, *24*(4), 905–921. doi: 10.1007/s10040-015-1358-7
- Allen, G. H., & Pavelsky, T. (2018). Global extent of rivers and streams. *Science*, *361*(6402), 585–588. doi: 10.1126/science.aat063
- Angelini, R., de Moraes, R. J., Catella, A. C., Resende, E. K., & Libralato, S. (2013). Aquatic food webs of the oxbow lakes in the Pantanal: A new site for fisheries guaranteed by alternated control? *Ecological Modelling*, *253*, 82–96. doi: 10.1016/j.ecolmodel.2013.01.001
- Aragón, R., Jobbágy, E. G., & Viglizzo, E. F. (2011). Surface and groundwater dynamics in the sedimentary plains of the Western Pampas (Argentina). *Ecohydrology*, *4*(3), 433–447. doi: 10.1002/eco.149
- Arias, P., Bellouin, N., Coppola, E., Jones, R., Krinner, G., Marotzke, J., . . . Zickfeld, K. (2021). *Technical summary* (Tech. Rep.). Geneva, Switzerland: The Intergovernmental Panel on Climate Change (IPCC).
- Blöschl, G., Kiss, A., Viglione, A., Barriendos, M., Böhm, O., Brázdil, R., . . . Wetter, O. (2020). Current European flood-rich period exceptional compared with past 500 years. *Nature*, *583*(7817), 560–566. doi: 10.1038/s41586-020-2478-3
- Brunsell, N. A. (2010). A multiscale information theory approach to assess spatial-temporal variability of daily precipitation. *Journal of Hydrology*, *385*(1-4), 165–172. doi: 10.1016/j.jhydrol.2010.02.016
- Buttle, J. M., Allen, D. M., Caissie, D., Davison, B., Hayashi, M., Peters, D. L., . . . Whitfield, P. H. (2016). Flood processes in Canada: Regional and special aspects. *Canadian Water Resources Journal / Revue canadienne des ressources hydriques*, *41*(1-2), 7–30. doi: 10.1080/07011784.2015.1131629

- 424 Camporeale, C., Perona, P., Porporato, A., & Ridolfi, L. (2005). On the long-term
425 behavior of meandering rivers. *Water Resources Research*, *41*(12). doi: 10
426 .1029/2005WR004109
- 427 Chakrapani, G. J. (2005). Factors controlling variations in river sediment loads.
428 *Current science*, 569–575.
- 429 Chen, C. F., Son, N. T., & Chang, L. Y. (2012). Monitoring of rice cropping inten-
430 sity in the upper Mekong Delta, Vietnam using time-series MODIS data. *Ad-
431 vances in Space Research*, *49*(2), 292–301. doi: 10.1016/j.asr.2011.09.011
- 432 Constantine, J. A., & Dunne, T. (2008). Meander cutoff and the controls on the pro-
433 duction of oxbow lakes. *Geology*, *36*(1), 23–26. doi: 10.1130/G24130A.1
- 434 Davidson, N. C., Fluet-Chouinard, E., & Finlayson, C. M. (2018). Global extent and
435 distribution of wetlands: Trends and issues. *Marine and Freshwater Research*,
436 *69*(4), 620–627. doi: 10.1071/MF17019
- 437 Dong, J., Xiao, X., Kou, W., Qin, Y., Zhang, G., Li, L., . . . Moore, B. (2015).
438 Tracking the dynamics of paddy rice planting area in 1986-2010 through time
439 series Landsat images and phenology-based algorithms. *Remote Sensing of
440 Environment*, *160*, 99–113. doi: 10.1016/j.rse.2015.01.004
- 441 Elith, J., Leathwick, J. R., & Hastie, T. (2008). *A working guide to boosted regres-
442 sion trees* (Vol. 77) (No. 4). John Wiley & Sons, Ltd. doi: 10.1111/j.1365-2656
443 .2008.01390.x
- 444 Ellis, E., & Klein Goldewijk, K. (2019). *Anthromes 12k full dataset* [dataset].
445 Retrieved from [https://dataverse.harvard.edu/dataset.xhtml](https://dataverse.harvard.edu/dataset.xhtml?persistentId=doi:10.7910/DVN/GOQDNQ)
446 [?persistentId=doi:10.7910/DVN/GOQDNQ](https://doi.org/10.7910/DVN/GOQDNQ) doi: 10.7910/DVN/GOQDNQ
- 447 Finotello, A., D’Alpaos, A., Bogoni, M., Ghinassi, M., & Lanzoni, S. (2020).
448 Remotely-sensed planform morphologies reveal fluvial and tidal nature
449 of meandering channels. *Scientific Reports 2020 10:1*, *10*(1), 1–13. doi:
450 10.1038/s41598-019-56992-w
- 451 Frasson, R. P. d. M., Pavelsky, T. M., Fonstad, M. A., Durand, M. T., Allen, G. H.,
452 Schumann, G., . . . Yang, X. (2019). *Global database of river width, slope,
453 catchment area, meander wavelength, sinuosity, and discharge* [dataset]. Zen-
454 odo. Retrieved from <https://doi.org/10.5281/zenodo.2582500> doi:
455 10.5281/zenodo.2582500
- 456 Gardner, J. R., Yang, X., Topp, S. N., Ross, M. R., Altenau, E. H., & Pavelsky,
457 T. M. (2021). The Color of Rivers. *Geophysical Research Letters*, *48*(1),
458 e2020GL088946. doi: 10.1029/2020GL088946
- 459 Gorelick, N., Hancher, M., Dixon, M., Ilyushchenko, S., Thau, D., & Moore, R.
460 (2017). Google Earth Engine: Planetary-scale geospatial analysis for everyone.
461 *Remote Sensing of Environment*, *202*, 18–27. doi: 10.1016/j.rse.2017.06.031
- 462 Griffin-Nolan, R. J., Slette, I. J., & Knapp, A. K. (2021). Deconstructing precipi-
463 tation variability: Rainfall event size and timing uniquely alter ecosystem dy-
464 namics. *Journal of Ecology*, *109*(9), 3356–3369. doi: 10.1111/1365-2745.13724
- 465 Houspanossian, J., Kuppel, S., Nosetto, M. D., Di Bella, C. M., Oricchio, P., Barru-
466 cand, M., . . . Jobbágy, E. G. (2018). Long-lasting floods buffer the thermal
467 regime of the Pampas. *Theoretical and Applied Climatology*, *131*(1-2), 111–
468 120. doi: 10.1007/s00704-016-1959-7
- 469 Junk, W., Bayley, P., & Sparks, R. (1989). The flood pulse concept in river-
470 floodplain systems. *Canadian Special Publication of Fisheries and Aquatic
471 Sciences*, *106*(Canadian Special Publication of Fisheries and Aquatic Sci-
472 ences), 110–127.
- 473 Kireeva, M. B., Rets, E. P., Frolova, N. L., Samsonov, T. E., Povalishnikova, E. S.,
474 Entin, A. L., . . . Ivanov, A. M. (2020). Occasional floods on the rivers of rus-
475 sian plain in the 20th –21st centuries. *Geography, Environment, Sustainability*,
476 *13*(2), 84–95. doi: 10.24057/2071-9388-2020-29
- 477 Kundzewicz, Z. W. (2008). Climate change impacts on the hydrological cycle. *Eco-
478 hydrology & Hydrobiology*, *8*(2-4), 195–203. doi: 10.2478/v10104-009-0015-y

- 479 Kuppel, S., Houspanossian, J., Nosetto, M. D., & Jobbágy, E. G. (2015). What
 480 does it take to flood the Pampas?: Lessons from a decade of strong hydro-
 481 logical fluctuations. *Water Resources Research*, *51*(4), 2937–2950. doi:
 482 10.1002/2015WR016966
- 483 Langhorst, T., & Pavelsky, T. (2023). Global Observations of Riverbank Erosion and
 484 Accretion From Landsat Imagery. *Journal of Geophysical Research: Earth Sur-
 485 face*, *128*(2), e2022JF006774. doi: 10.1029/2022JF006774
- 486 Lehner, B., & Döll, P. (2004). Development and validation of a global database of
 487 lakes, reservoirs and wetlands. *Journal of Hydrology*, *296*(1-4), 1–22. doi: 10
 488 .1016/j.jhydrol.2004.03.028
- 489 Lehner, B., & Döll, P. (2004). *Global lakes and wetlands database: Lakes and
 490 wetlands grid (level 3)* [dataset]. World Wildlife Fund. Retrieved from
 491 [https://www.worldwildlife.org/publications/global-lakes-and-
 492 -wetlands-database-lakes-and-wetlands-grid-level-3](https://www.worldwildlife.org/publications/global-lakes-and-wetlands-database-lakes-and-wetlands-grid-level-3)
- 493 Lin, P., Pan, M., Allen, G. H., de Frasson, R. P., Zeng, Z., Yamazaki, D., & Wood,
 494 E. F. (2020). Global Estimates of Reach-Level Bankfull River Width Lever-
 495 aging Big Data Geospatial Analysis. *Geophysical Research Letters*, *47*(7),
 496 e2019GL086405. doi: 10.1029/2019GL086405
- 497 Liu, G. (2022). Understanding cotton cultivation dynamics in Aksu Oases (NW
 498 China) by reconstructing change trajectories using multi-temporal Land-
 499 sat and Sentinel-2 data. *Geocarto International*, *37*(15), 4406–4424. doi:
 500 10.1080/10106049.2021.1886337
- 501 Loarie, S. R., Lobell, D. B., Asner, G. P., & Field, C. B. (2011). Land-Cover and
 502 Surface Water Change Drive Large Albedo Increases in South America*. *Earth
 503 Interactions*, *15*(7), 1–16. doi: 10.1175/2010EI342.1
- 504 McGuire, K. J., McDonnell, J. J., Weiler, M., Kendall, C., McGlynn, B. L.,
 505 Welker, J. M., & Seibert, J. (2005). The role of topography on catchment-
 506 scale water residence time. *Water Resources Research*, *41*(5), 1–14. doi:
 507 10.1029/2004WR003657
- 508 Najibi, N., & Devineni, N. (2018). Recent trends in the frequency and duration of
 509 global floods. *Earth System Dynamics*, *9*(2), 757–783. doi: 10.5194/esd-9-757
 510 -2018
- 511 Olthof, I., & Rainville, T. (2022). Dynamic surface water maps of Canada from
 512 1984 to 2019 Landsat satellite imagery. *Remote Sensing of Environment*, *279*,
 513 113121. doi: 10.1016/J.RSE.2022.113121
- 514 Opperman, J. J., Luster, R., McKenney, B. A., Roberts, M., & Meadows, A. W.
 515 (2010). Ecologically functional floodplains: Connectivity, flow regime, and
 516 scale. *Journal of the American Water Resources Association*, *46*(2), 211–226.
 517 doi: 10.1111/j.1752-1688.2010.00426.x
- 518 Papa, F., Güntner, A., Frappart, F., Prigent, C., & Rossow, W. B. (2008). Varia-
 519 tions of surface water extent and water storage in large river basins: A com-
 520 parison of different global data sources. *Geophysical Research Letters*, *35*(11),
 521 L11401. doi: 10.1029/2008GL033857
- 522 Papa, F., Prigent, C., Aires, F., Jimenez, C., Rossow, W. B., & Matthews, E.
 523 (2010). Interannual variability of surface water extent at the global scale,
 524 1993–2004. *Journal of Geophysical Research*, *115*(D12), D12111. doi:
 525 10.1029/2009JD012674
- 526 Pekel, J.-F., Cottam, A., Gorelick, N., & Belward, A. S. (2016a). High-resolution
 527 mapping of global surface water and its long-term changes. *Nature*, *540*(7633),
 528 418–422. doi: 10.1038/nature20584
- 529 Pekel, J.-F., Cottam, A., Gorelick, N., & Belward, A. S. (2016b). *High-resolution
 530 mapping of global surface water and its long-term changes* [dataset]. Na-
 531 ture Publishing Group. Retrieved from [https://developers.google.com/
 532 earth-engine/datasets/catalog/JRC_GSW1_4_MonthlyHistory](https://developers.google.com/earth-engine/datasets/catalog/JRC_GSW1_4_MonthlyHistory) doi:
 533 10.1038/nature20584

- 534 Pi, X., Luo, Q., Feng, L., Xu, Y., Tang, J., Liang, X., . . . Bryan, B. A. (2022). Map-
 535 ping global lake dynamics reveals the emerging roles of small lakes. *Nature*
 536 *Communications*, *13*(1), 1–12. doi: 10.1038/s41467-022-33239-3
- 537 Pickens, A. H., Hansen, M. C., Hancher, M., Stehman, S. V., Tyukavina, A.,
 538 Potapov, P., . . . Sherani, Z. (2020). Mapping and sampling to character-
 539 ize global inland water dynamics from 1999 to 2018 with full Landsat time-
 540 series. *Remote Sensing of Environment*, *243*(December 2019), 111792. doi:
 541 10.1016/j.rse.2020.111792
- 542 Poole, G. C. (2010). Stream hydrogeomorphology as a physical science basis for ad-
 543 vances in stream ecology. *Journal of the North American Benthological Society*,
 544 *29*(1), 12–25. doi: 10.1899/08-070.1
- 545 R Core Team. (2021). R: A language and environment for statistical computing
 546 [Computer software manual]. Vienna, Austria. Retrieved from [https://www.R-](https://www.R-project.org/)
 547 [project.org/](https://www.R-project.org/)
- 548 Radinger, J., Alcaraz-Hernández, J. D., & García-Berthou, E. (2018). Environ-
 549 mental and spatial correlates of hydrologic alteration in a large Mediterranean
 550 river catchment. *Science of The Total Environment*, *639*, 1138–1147. doi:
 551 10.1016/J.SCITOTENV.2018.05.227
- 552 Richardson, J., Sangree, J., & Sneider, R. (1987). Meandering Stream Reservoirs.
 553 *Journal of Petroleum Technology*, *39*(12), 1501–1502. doi: 10.2118/15781-PA
- 554 Riley, S., DeGloria, S., & Elliot, R. (1999). A terrain ruggedness that quantifies to-
 555 pographic heterogeneity. *Intermountain Journal of Science*, *5*(1-4), 23–27.
- 556 Rudorff, C. M., Melack, J. M., & Bates, P. D. (2014). Flooding dynamics on the
 557 lower Amazon floodplain: 1. Hydraulic controls on water elevation, inunda-
 558 tion extent, and river-floodplain discharge. *Water Resources Research*, *50*(1),
 559 619–634. doi: 10.1002/2013WR014091
- 560 Sakamoto, T., Van Nguyen, N., Kotera, A., Ohno, H., Ishitsuka, N., & Yokozawa,
 561 M. (2007). Detecting temporal changes in the extent of annual flood-
 562 ing within the Cambodia and the Vietnamese Mekong Delta from MODIS
 563 time-series imagery. *Remote Sensing of Environment*, *109*(3), 295–313. doi:
 564 10.1016/j.rse.2007.01.011
- 565 Saunio, M., Stavert, A. R., Poulter, B., Bousquet, P., Canadell, J. G., Jackson,
 566 R. B., . . . Zhuang, Q. (2020). The Global Methane Budget 2000–2017. *Earth*
 567 *System Science Data*, *12*(3), 1561–1623. doi: 10.5194/essd-12-1561-2020
- 568 Siebert, S., Kummu, M., Porkka, M., Döll, P., Ramankutty, N., & Scanlon,
 569 B. R. (2015). A global data set of the extent of irrigated land from 1900
 570 to 2005. *Hydrology and Earth System Sciences*, *19*(3), 1521–1545. doi:
 571 10.5194/hess-19-1521-2015
- 572 Sivapalan, M., Thompson, S. E., Harman, C. J., Basu, N. B., & Kumar, P.
 573 (2011). Water cycle dynamics in a changing environment: Improving pre-
 574 dictability through synthesis. *Water Resources Research*, *47*(10). doi:
 575 10.1029/2011WR011377
- 576 Tena, A., Piégay, H., Seignemartin, G., Barra, A., Berger, J. F., Mourier, B., &
 577 Winiarski, T. (2020). Cumulative effects of channel correction and regulation
 578 on floodplain terrestrialisation patterns and connectivity. *Geomorphology*, *354*.
 579 doi: 10.1016/j.geomorph.2020.107034
- 580 Tockner, K., Malard, F., & Ward, J. V. (2000). An extension of the flood pulse
 581 concept. *Hydrological Processes*, *14*(16-17), 2861–2883. doi: 10.1002/1099-
 582 -1085(200011/12)14:16/17<2861::AID-HYP124>3.0.CO;2-F
- 583 Tockner, K., & Stanford, J. A. (2002). Riverine flood plains: Present state and
 584 future trends. *Environmental Conservation*, *29*(3), 308–330. doi: 10.1017/
 585 S037689290200022X
- 586 Tooth, S. (2000). Process, form and change in dryland rivers: A review of recent re-
 587 search. *Earth Science Reviews*, *51*(1-4), 67–107. doi: 10.1016/S0012-8252(00)
 588 00014-3

- 589 Torre Zaffaroni, P., Baldi, G., Texeira, M., Di Bella, C. M., & Jobbagy, E. G.
 590 (2023). The timing of global floods and its association with climate and to-
 591 pography. *ESS Open Archive*. doi: 10.1002/essoar.10511955.2
- 592 Tran, D. D., van Halsema, G., Hellegers, P. J., Ludwig, F., & Wyatt, A. (2018).
 593 Questioning triple rice intensification on the Vietnamese mekong delta flood-
 594 plains: An environmental and economic analysis of current land-use trends
 595 and alternatives. *Journal of Environmental Management*, 217, 429–441. doi:
 596 10.1016/j.jenvman.2018.03.116
- 597 Twine, T. E., Kucharik, C. J., & Foley, J. A. (2004). Effects of Land Cover Change
 598 on the Energy and Water Balance of the Mississippi River Basin. *Journal*
 599 *of Hydrometeorology*, 5(4), 640–655. doi: 10.1175/1525-7541(2004)005<0640:
 600 EOLCCO>2.0.CO;2
- 601 Van Dijk, W. M., Van de Lageweg, W. I., & Kleinhans, M. G. (2013). Formation of
 602 a cohesive floodplain in a dynamic experimental meandering river. *Earth Sur-*
 603 *face Processes and Landforms*, 38(13), 1550–1565. doi: 10.1002/ESP.3400
- 604 Vörösmarty, C. J., McIntyre, P. B., Gessner, M. O., Dudgeon, D., Prusevich, A.,
 605 Green, P., . . . Davies, P. M. (2010). Global threats to human water security
 606 and river biodiversity. *Nature*, 467(7315), 555–561. doi: 10.1038/nature09440
- 607 Walcker, R., Corenblit, D., Julien, F., Martinez, J.-M., & Steiger, J. (2021). Con-
 608 tribution of meandering rivers to natural carbon fluxes: Evidence from the
 609 Ucayali River, Peruvian Amazonia. *Science of The Total Environment*, 776,
 610 146056. doi: 10.1016/j.scitotenv.2021.146056
- 611 Wantzen, K. M., Junk, W. J., & Rothhaupt, K.-O. (2008). An extension of the
 612 floodpulse concept (FPC) for lakes. In *Ecological effects of water-level fluctua-*
 613 *tions in lakes* (pp. 151–170). Dordrecht: Springer Netherlands. doi: 10.1007/
 614 978-1-4020-9192-6_15
- 615 Ward, J. V., & Stanford, J. A. (1995). Ecological connectivity in alluvial river
 616 ecosystems and its disruption by flow regulation. *Regulated Rivers: Research &*
 617 *Management*, 11(1), 105–119. doi: 10.1002/rrr.3450110109
- 618 Watts, J. D., Kimball, J. S., Bartsch, A., & McDonald, K. C. (2014). Sur-
 619 face water inundation in the boreal-Arctic: Potential impacts on regional
 620 methane emissions. *Environmental Research Letters*, 9(7), 075001. doi:
 621 10.1088/1748-9326/9/7/075001
- 622 Wren, D. G., Davidson, G. R., Walker, W. G., & Galicki, S. J. (2008). The evolution
 623 of an oxbow lake in the Mississippi alluvial floodplain. *Journal of Soil and Wa-*
 624 *ter Conservation*, 63(3), 129–135. doi: 10.2489/jswc.63.3.129
- 625 Wu, J., Zhang, Q., Li, Y., Xu, C. Y., & Ye, X. (2023). Spatial-temporal variations of
 626 stage-area hysteretic relationships in large heterogeneous lake–floodplain sys-
 627 tems. *Journal of Hydrology*, 620, 129507. doi: 10.1016/j.jhydrol.2023.129507
- 628 Zeng, Z.-H., Lu, Z.-Y., Jiang, Y., Zhang, K., Yang, Y.-D., & Zhao, P.-Y. (2016).
 629 Legume-cereal crop rotation systems in china. *Crop Rotations: Farming Prac-*
 630 *tices, Monitoring and Environmental Benefits*. Ottawa, ON, Canada: Nova
 631 Science Publishers, 51–70.

Figure 1.

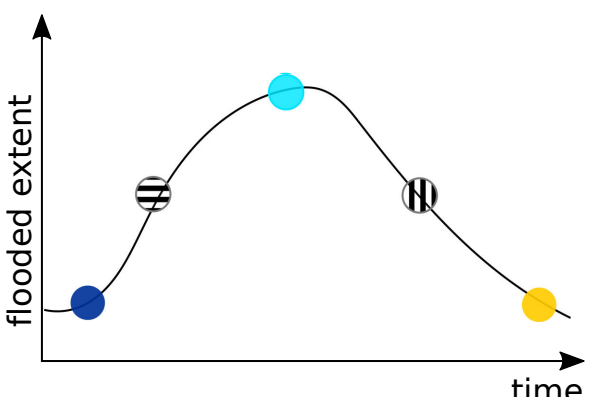
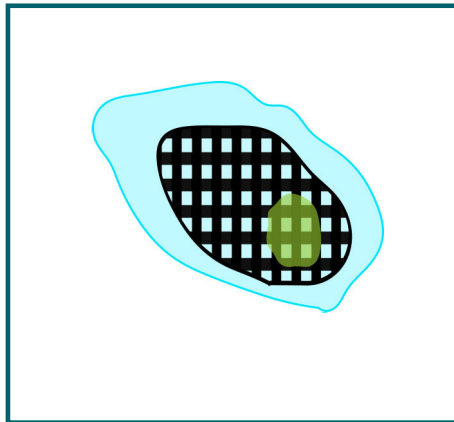
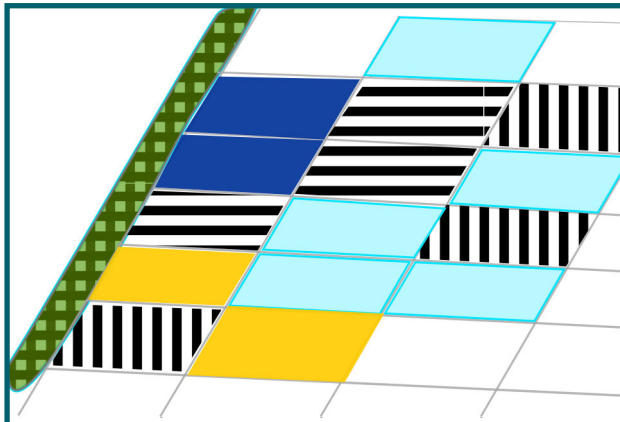
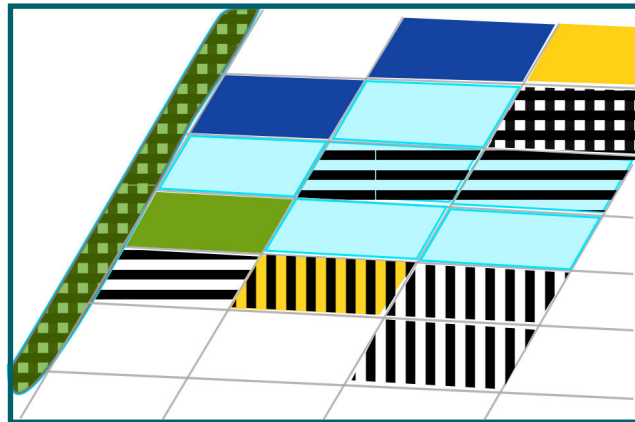
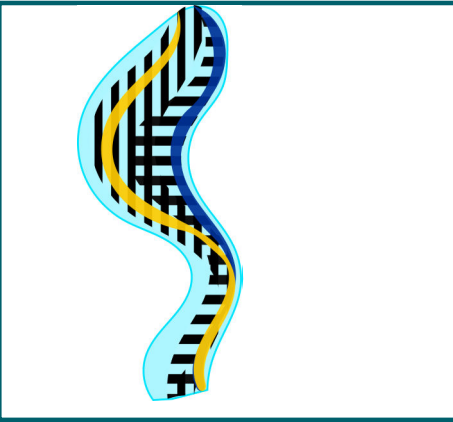
a)	b) case 1	c) case 2	d) case 3	e) case 4
				
is the variability spatially coherent?	Y	N	N	N
is the <i>extreme displacement</i> index (<i>dext</i>) able to capture the displacement?		Y	Y, but underestimates	N
is the <i>total displacement</i> index (<i>dtot</i>) able to capture the displacement?		Y	Y	Y

Figure 2.

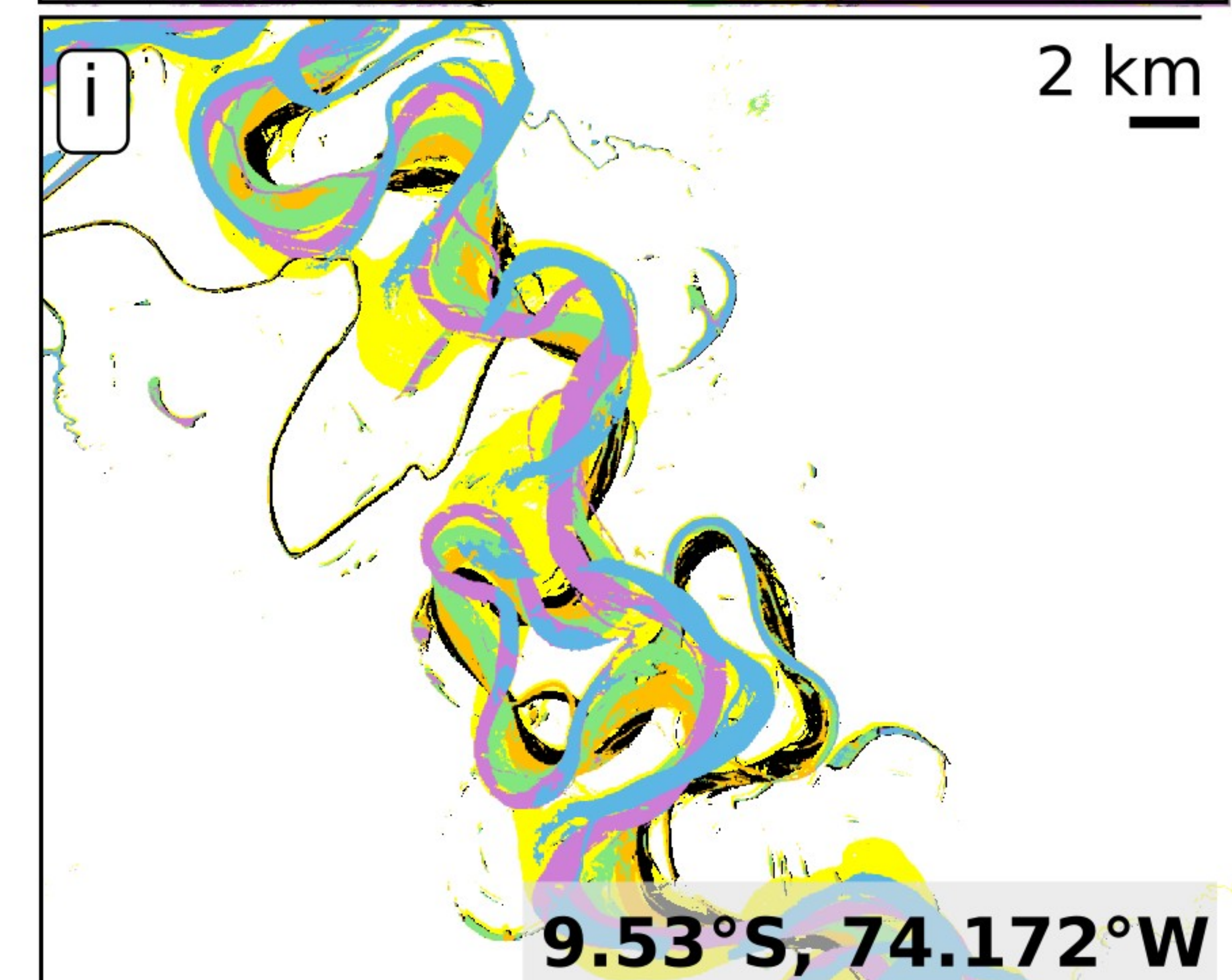
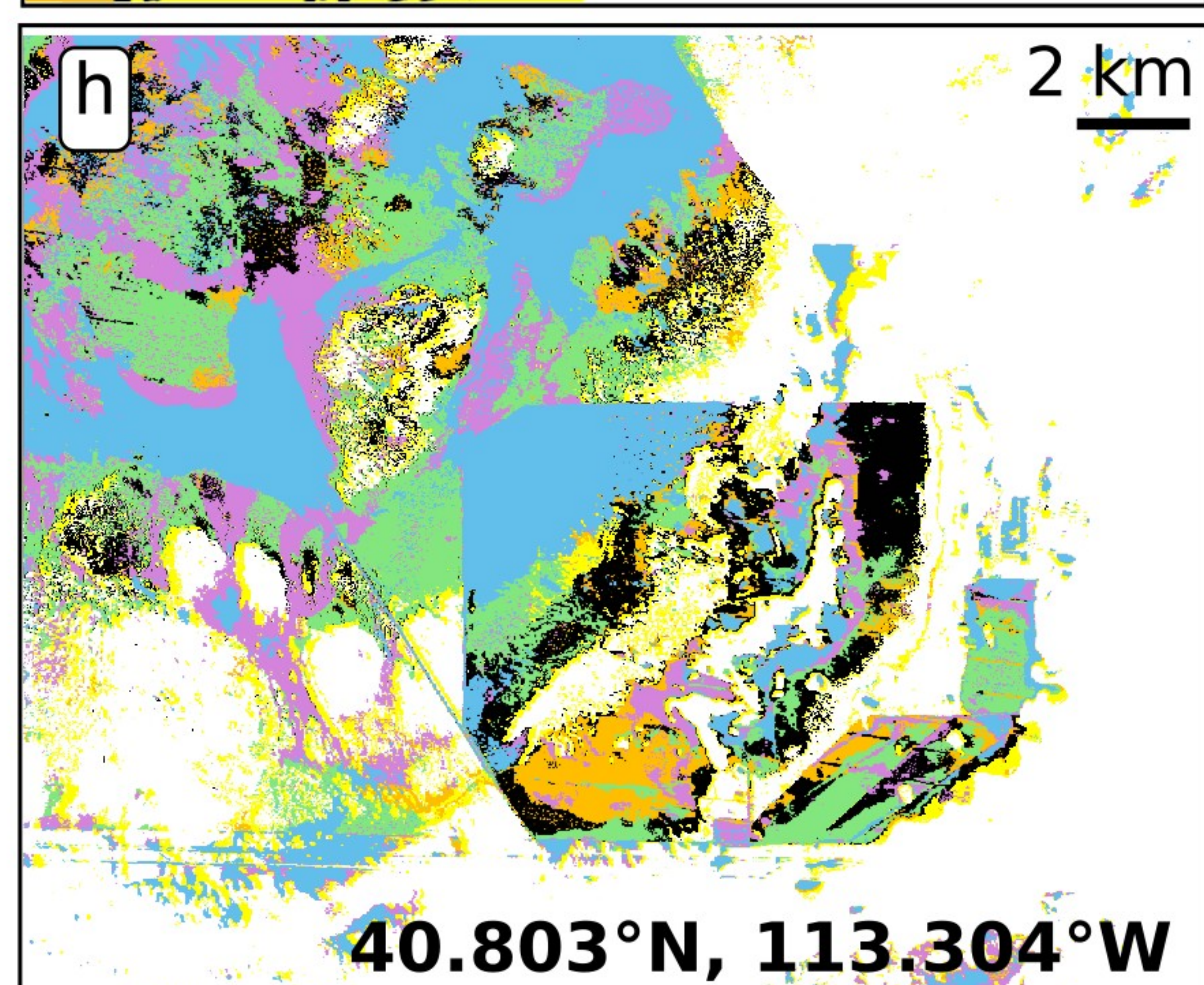
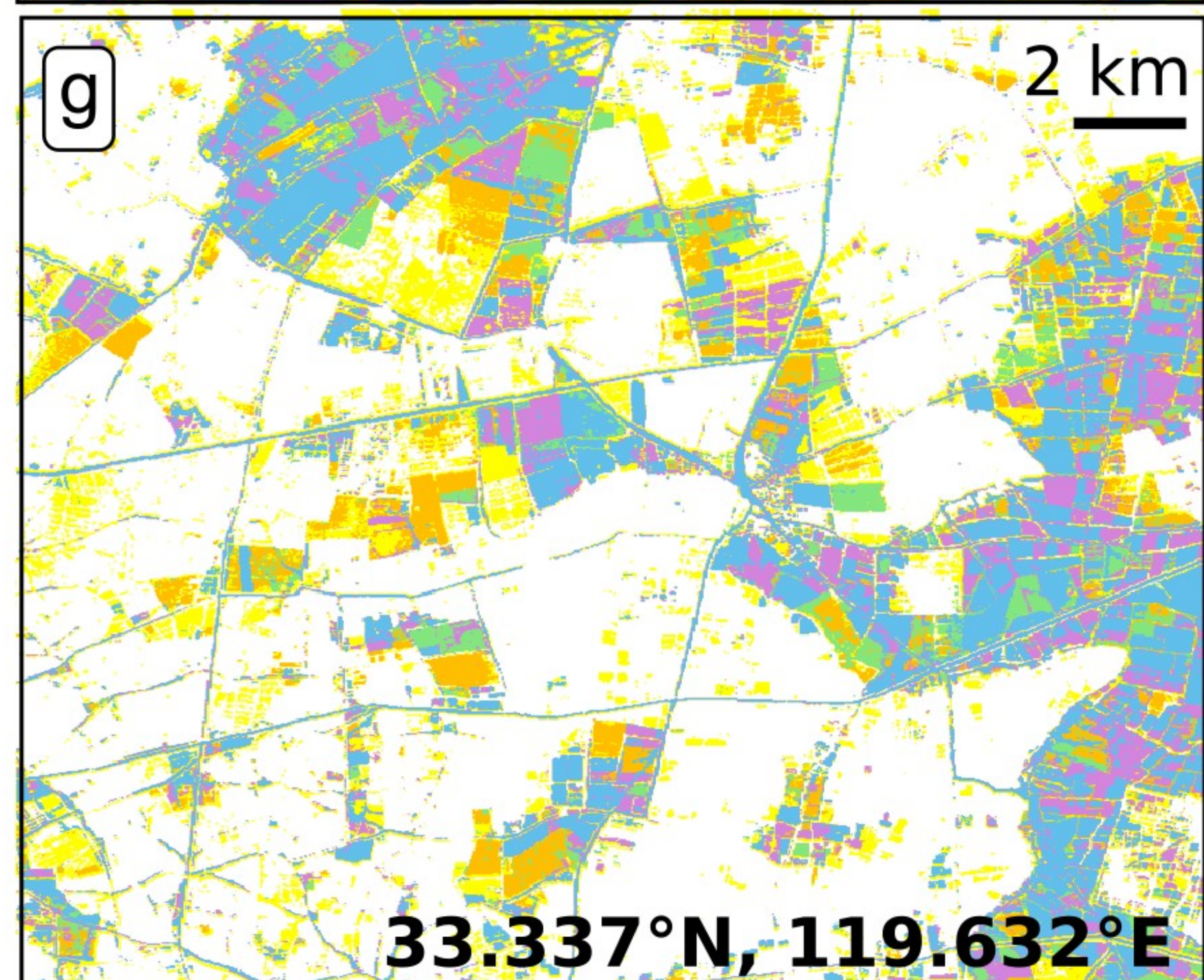
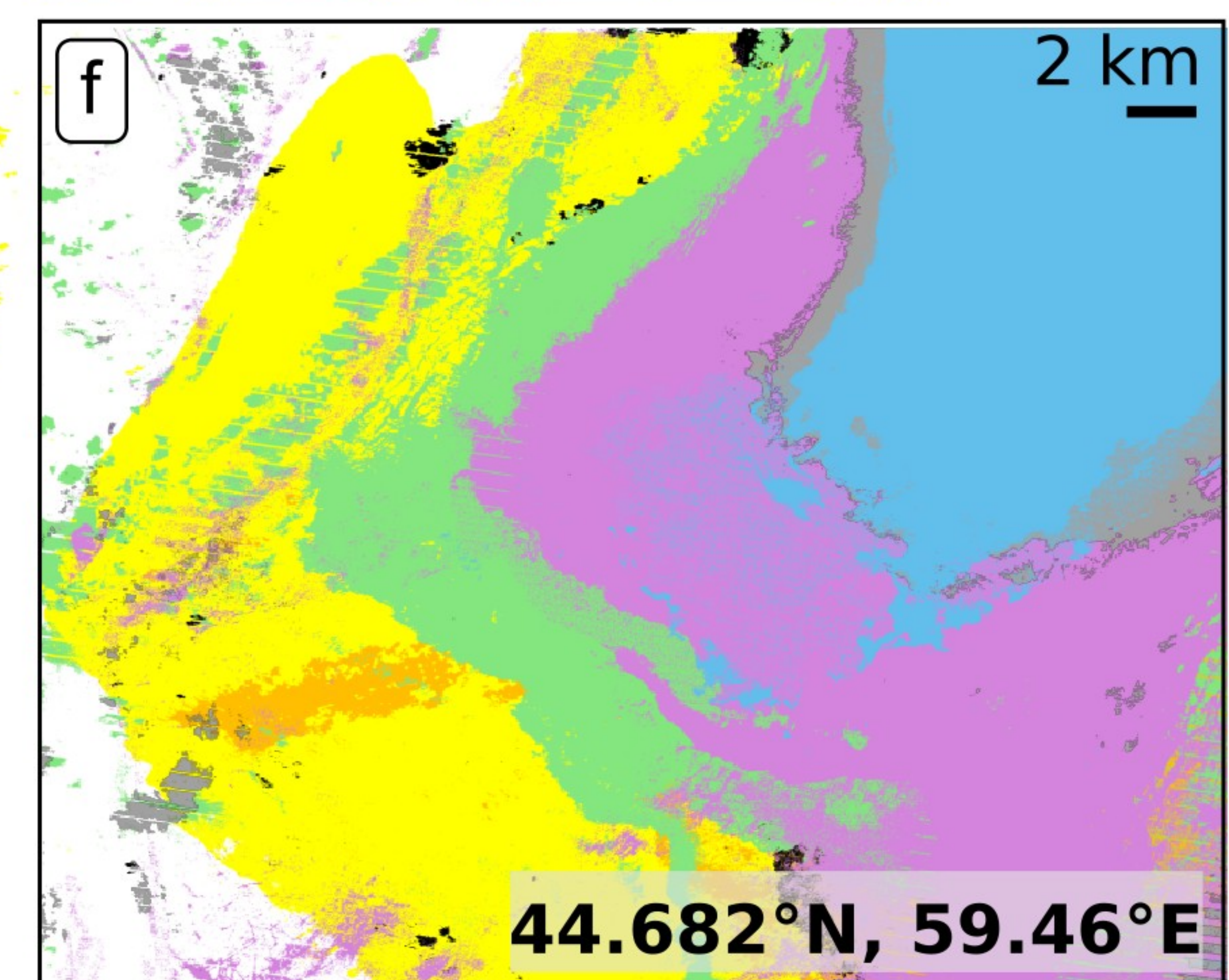
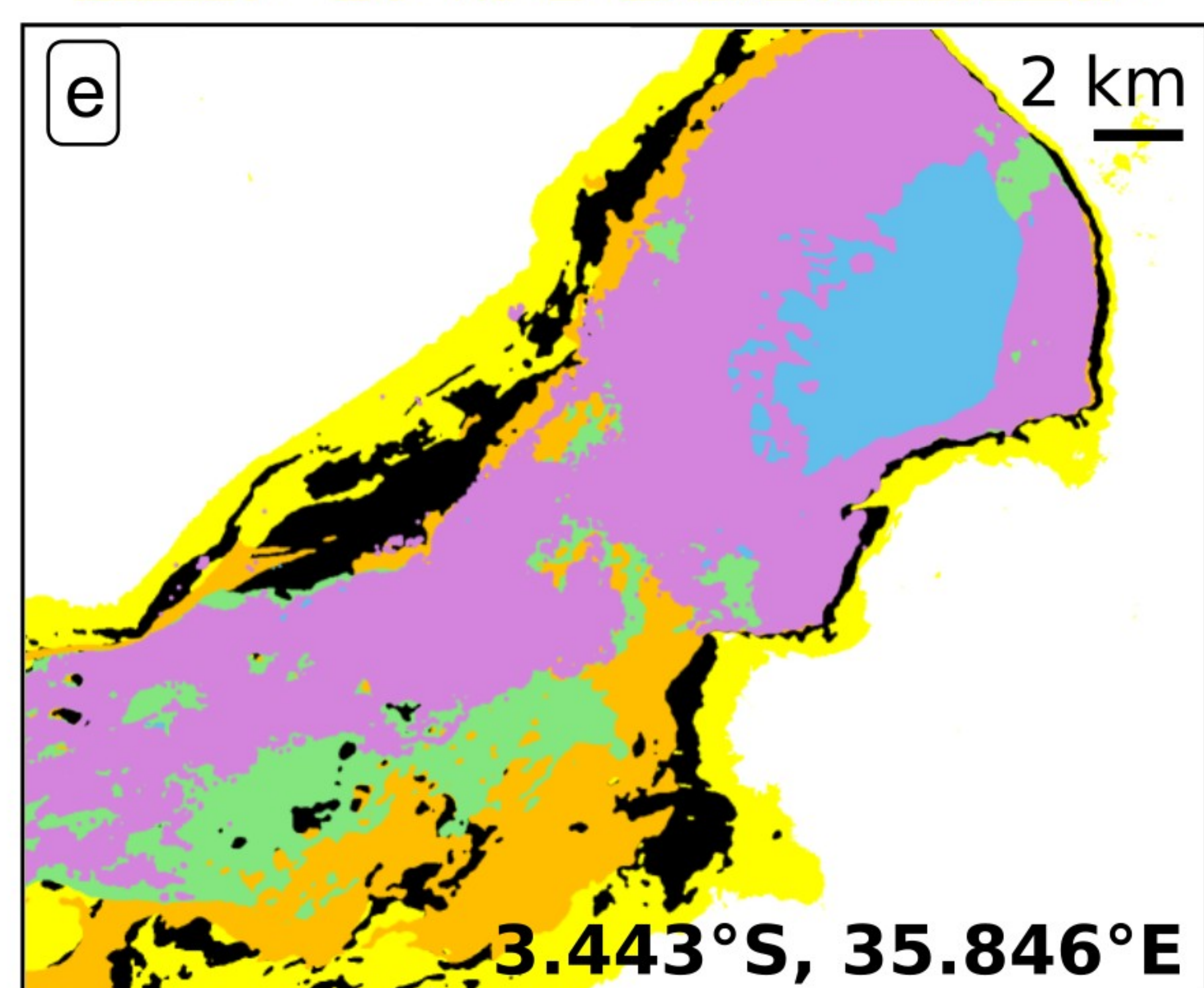
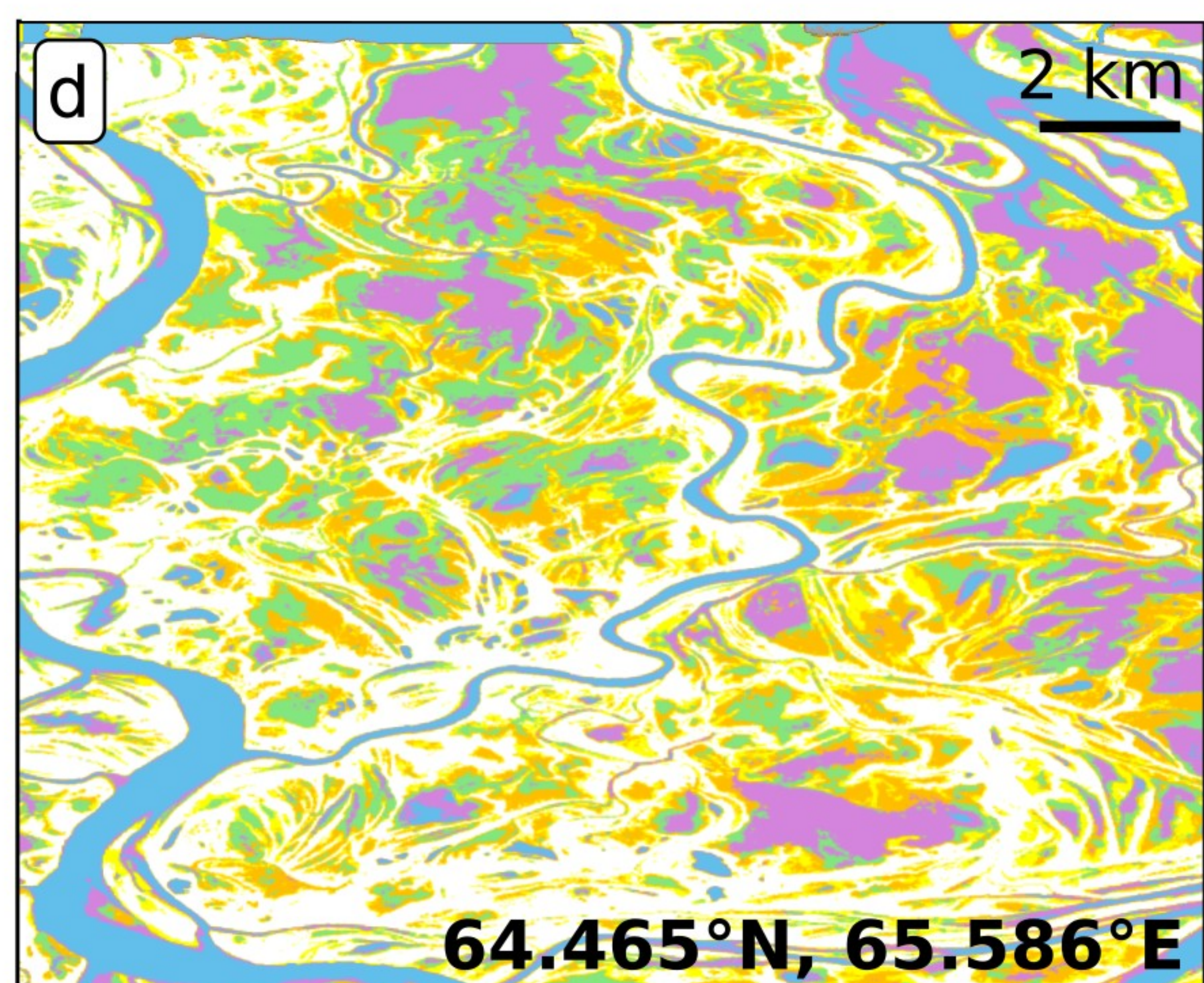
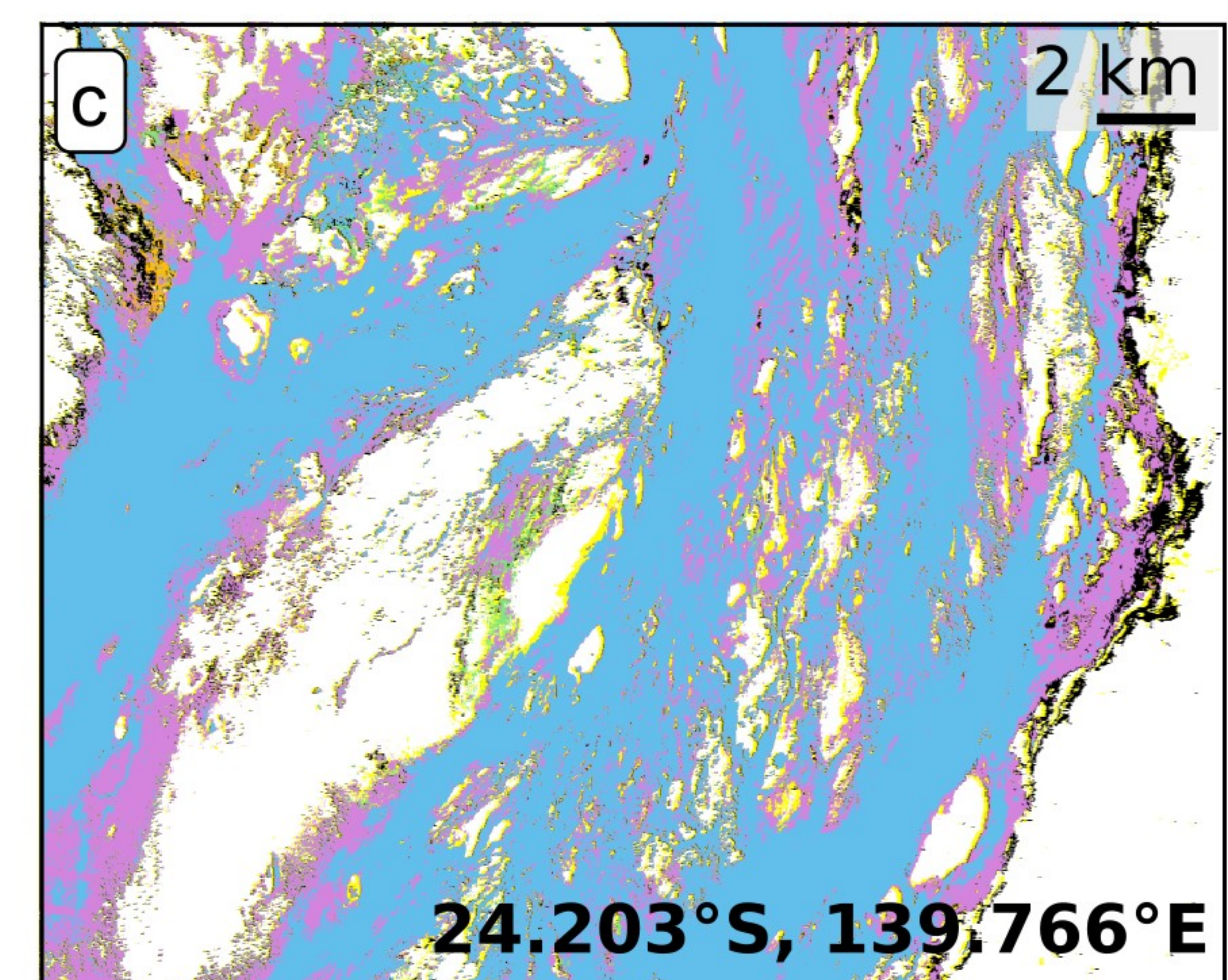
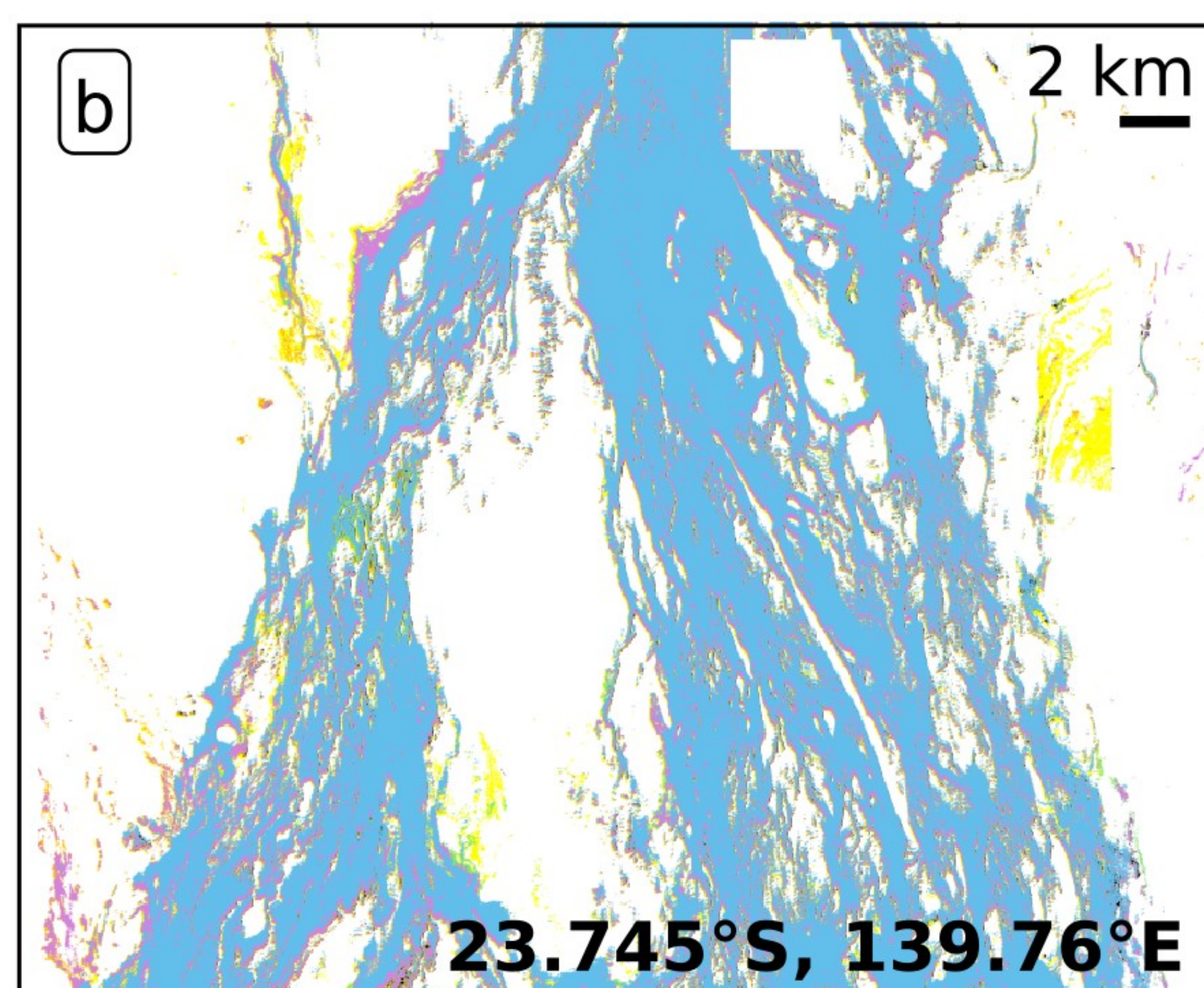
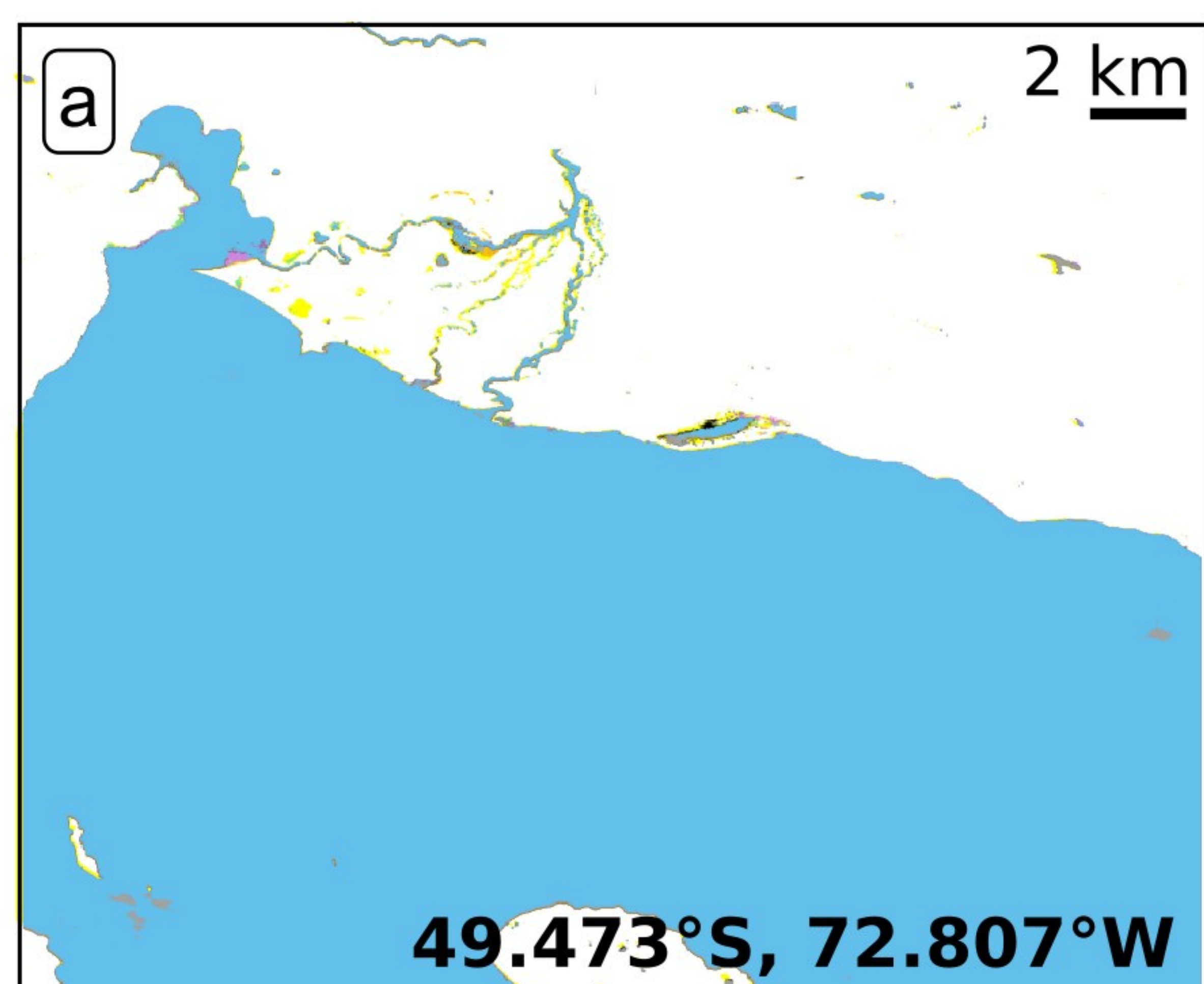
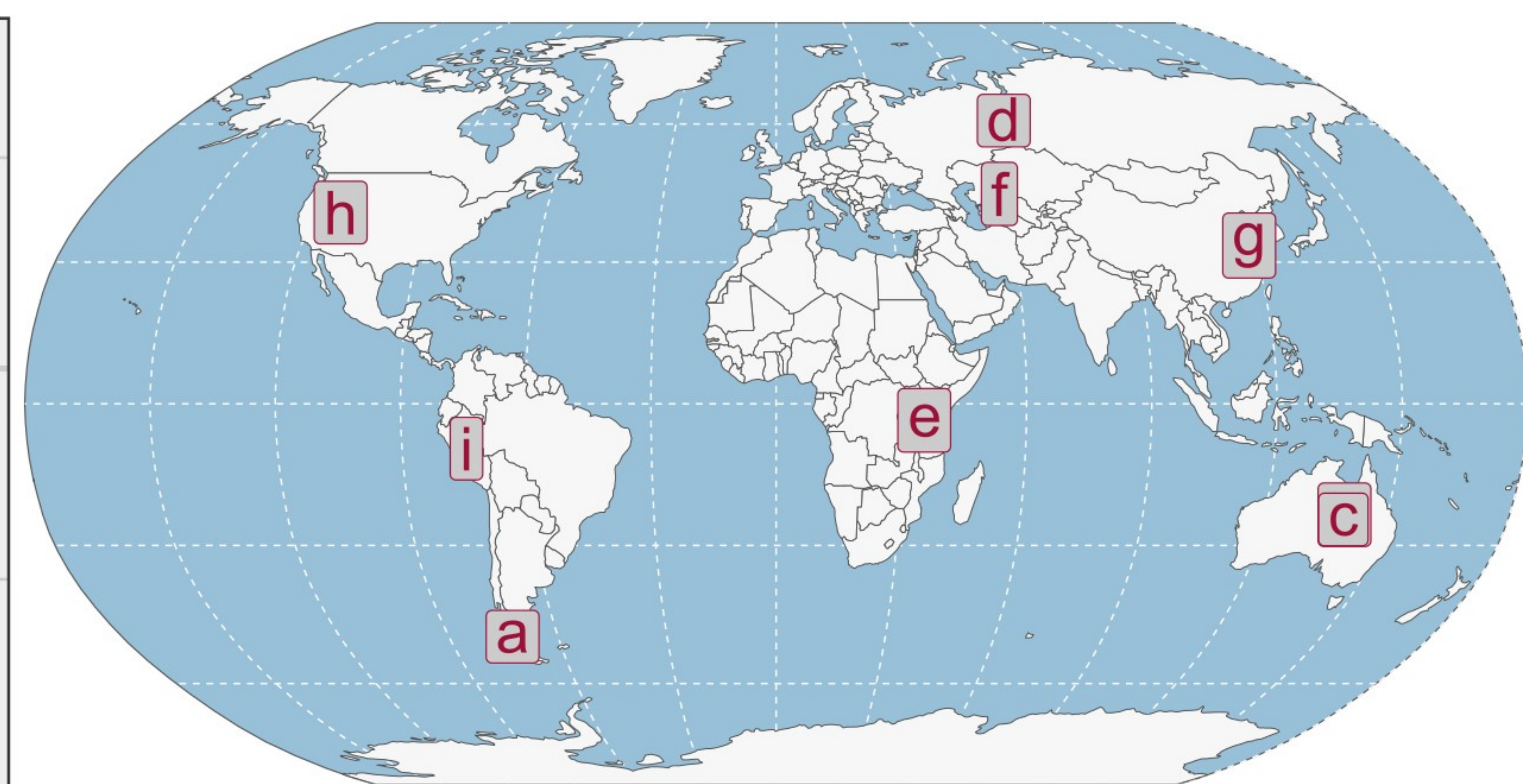
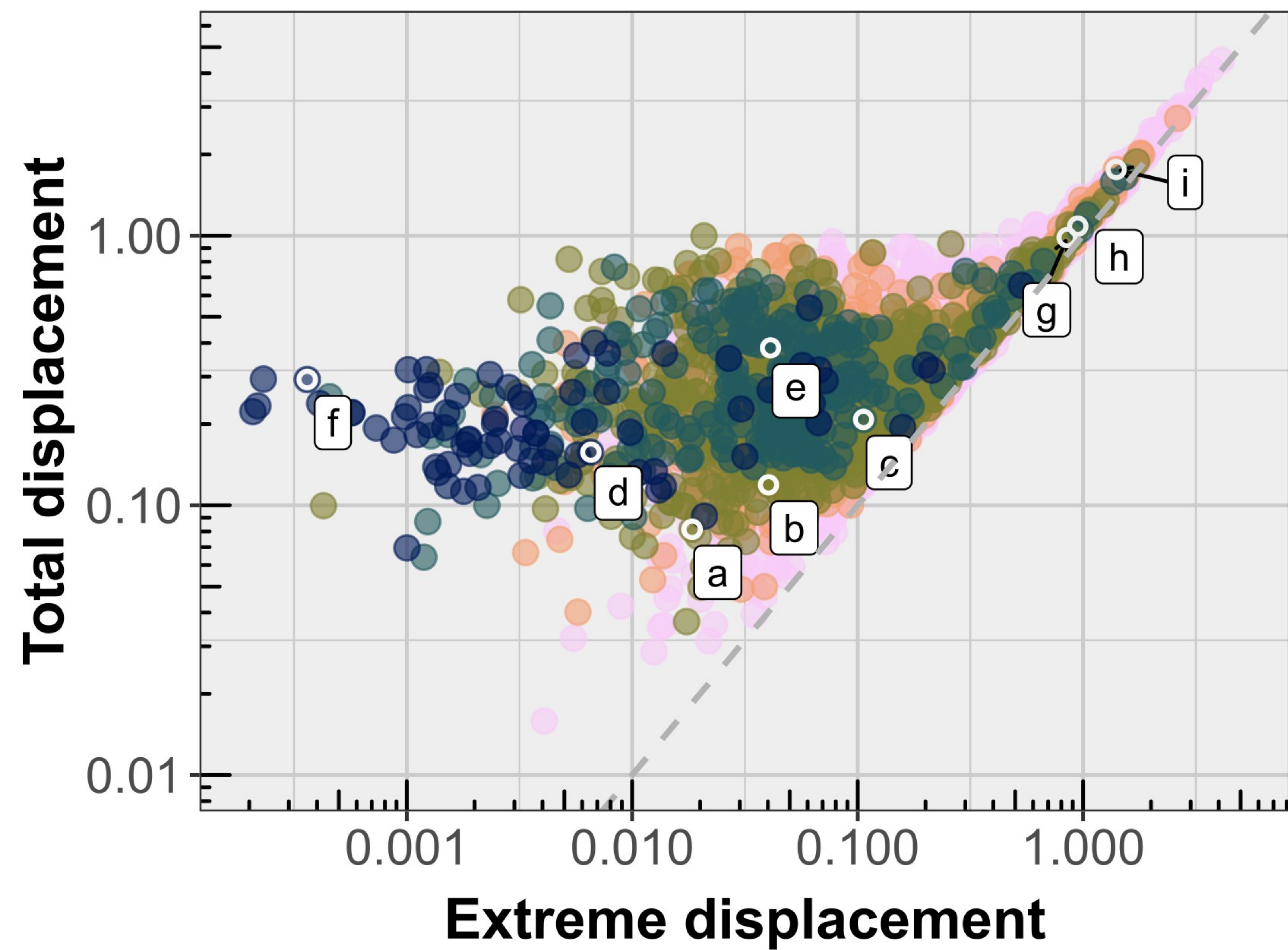
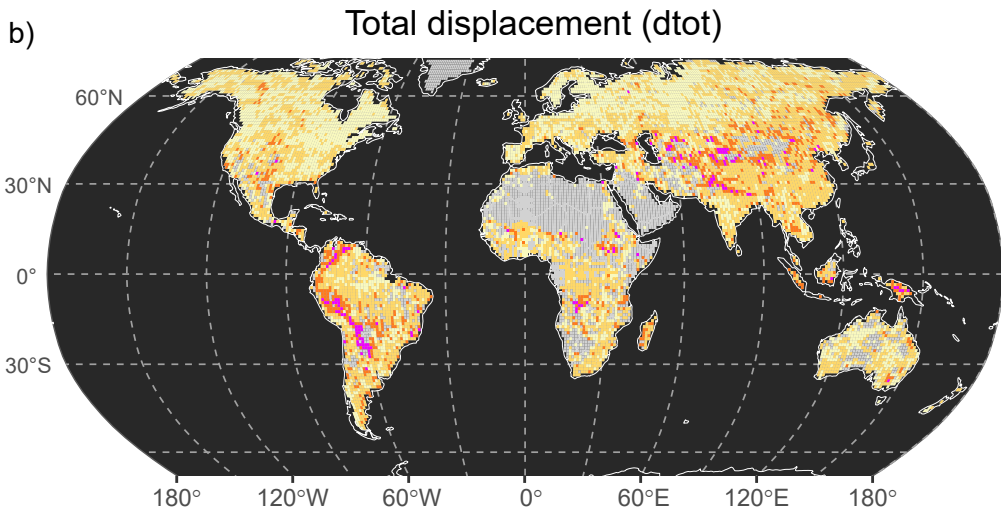
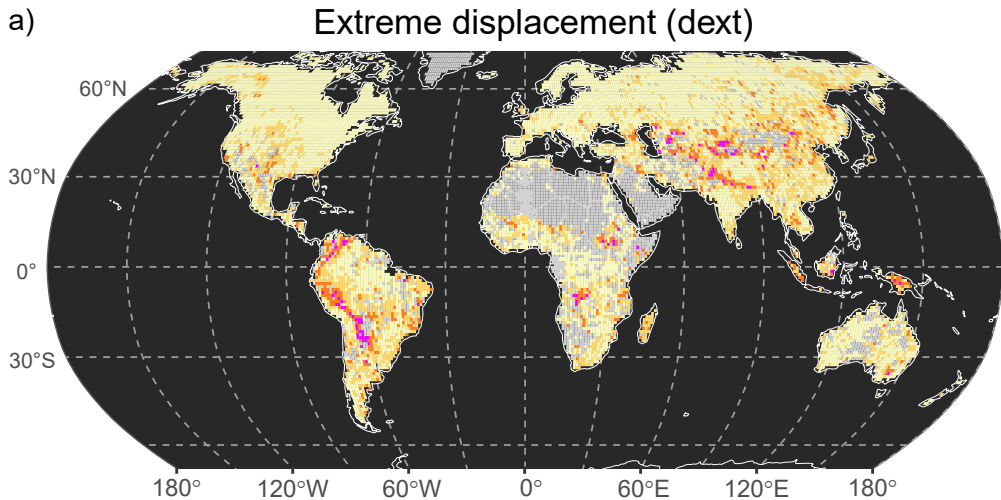


Figure 3.



Displacement



Geophysical Research Letters

Supporting Information for

Quantifying water cover shifts across the globe: following the steps of walking floods

P. Torre Zaffaroni^{1,2,3}, J. Houspanossian³, C.M. Di Bella^{1,2}, E.G. Jobbágy³

¹ Instituto de Investigaciones Fisiológicas y Ecológicas Vinculadas a la Agricultura (IFEVA), Facultad de Agronomía, Universidad de Buenos Aires, CONICET, Buenos Aires, Argentina

² Departamento de Métodos Cuantitativos y Sistemas de Información, Facultad de Agronomía, Universidad de Buenos Aires, Argentina

³ Grupo de Estudios Ambientales — IMASL, Universidad Nacional de San Luis & CONICET, San Luis, Argentina

Contents of this file

Text S1

Figures S1 to S6

Text S1.

Attribution of displacement to natural and induced factors

One way to test the influence of multiple continuous variables that might have interactive and/or non-linear effects is through boosted regression trees, which are based on machine learning algorithms capable of determining features' importance while maintaining adequate interpretability (Elith et al., 2008; Radinger et al., 2018). Based on the effect of topography on potential energy guiding the stagnancy of surface water, and of climate regimes in terms of spatial variability of rainfall events, we hypothesized that (1) displacement is fostered by low water convergence, which could be the result of largely flat topographies, highly meandering rivers, increasing aridity. Based on the different allocation of flooding for crops, decoupled from how flooding spreads over a floodplain, and the long-term effect of dam emplacement on the local flooding regime of the altered water course, we further hypothesize that (2) flooding displacement is enhanced by intensely irrigated regions destined to rice production and countered by well-defined lakes, including natural formations and manmade dams and emplacements for storing water.

We selected global datasets related to some of the most relevant aspects in which flooding displacement may be influenced by topography, climate, and large-scale anthropic activity. Figure S1 gathers the geographical distribution of these variables aggregated to each landscape. We obtained information from (1) Global Multi-resolution Terrain Elevation Data (GMTED2010, USGS) to derive three topographical variables: (a) terrain ruggedness (Riley et al., 1999), and slope integrated at (b) local (250m) and (c) regional (5km) levels (Figure S1 a-b); (2) Global database of river width, slope, catchment area, meander wavelength, sinuosity, and discharge (Frasson et al., 2019, and based upon Global River Width from Landsat, Allen & Pavelsky 2018) to derive the average meander wavelength across all riverine segments (between 60°N and 56°S) contained in each landscape (Figure S1c); (3) Global Lake and Wetlands Dataset (GLWD; Lehner & Doll 2004) to derive four hydrological variables: lake, river, floodplain and reservoir coverage fractions per landscape (Figure S1 d-g); (4) TerraClimate (Abatzoglou et al., 2018) to derive the climatological aridity index as the long-term of annual precipitation-to-potential evapotranspiration ratio (Figure S1h); (5) 2015 Anthromes 12K (Ellis et al., 2019) from which we derived three agricultural variables related with water management: rice, irrigated and rainfed coverage fractions per landscape (Figure S1 i-k). We also included the fraction covered by remote woodlands and flooded forests (Figure S1 l-m) as a proxy of one key passive satellite data caveat which can interfere with the depiction of surface water observation by remote sensors onboard satellite platforms.

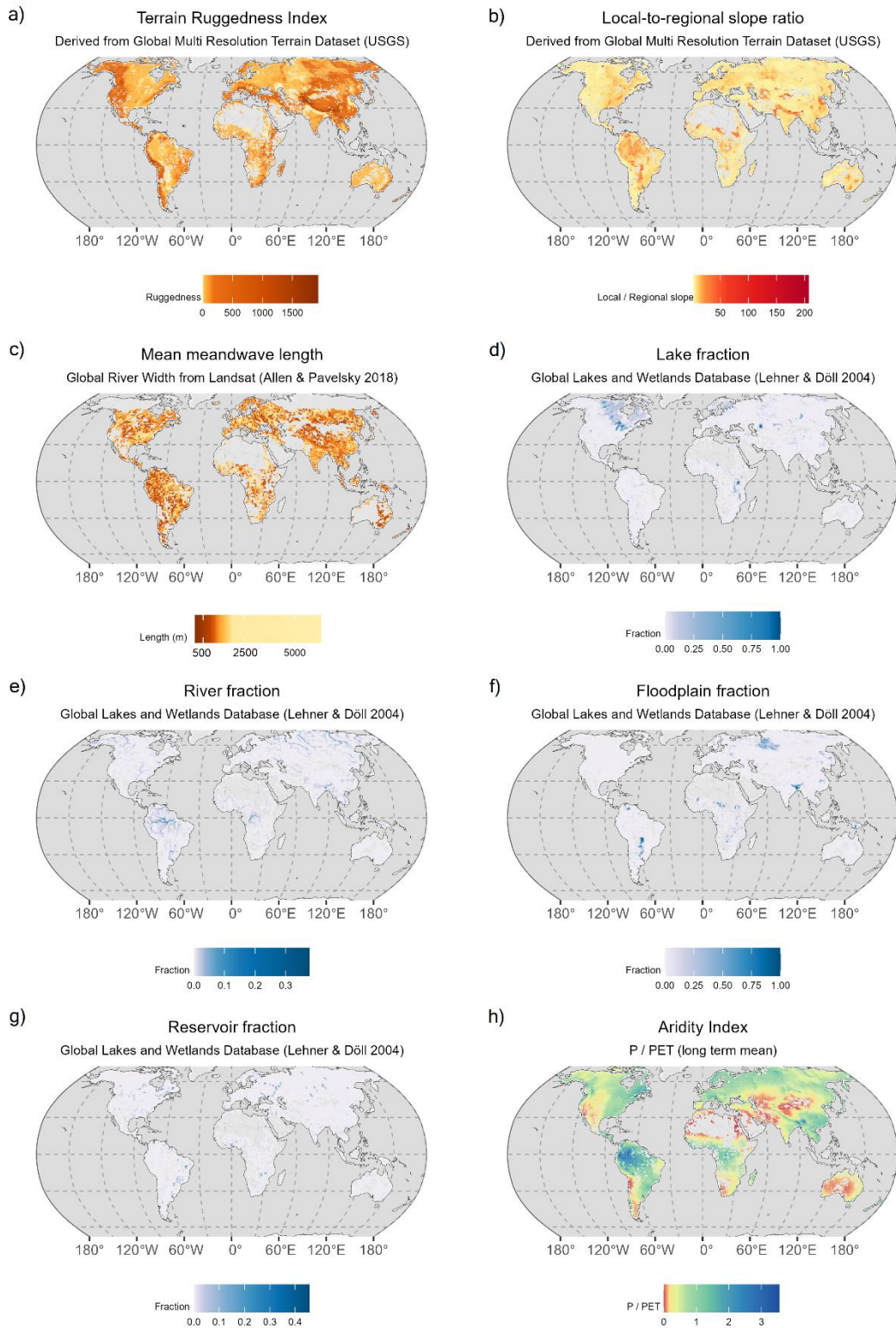


Figure S1. Geographical distribution of the thirteen variables for which we analyzed their influence on flooding displacement: (a) Terrain Ruggedness Index; (b) Local-to-Regional slope ratio; (c) Mean meandwave length; (d) Lake fraction; (e) River fraction; (f) Floodplain fraction; (g) Reservoir fraction; (h) Aridity Index.

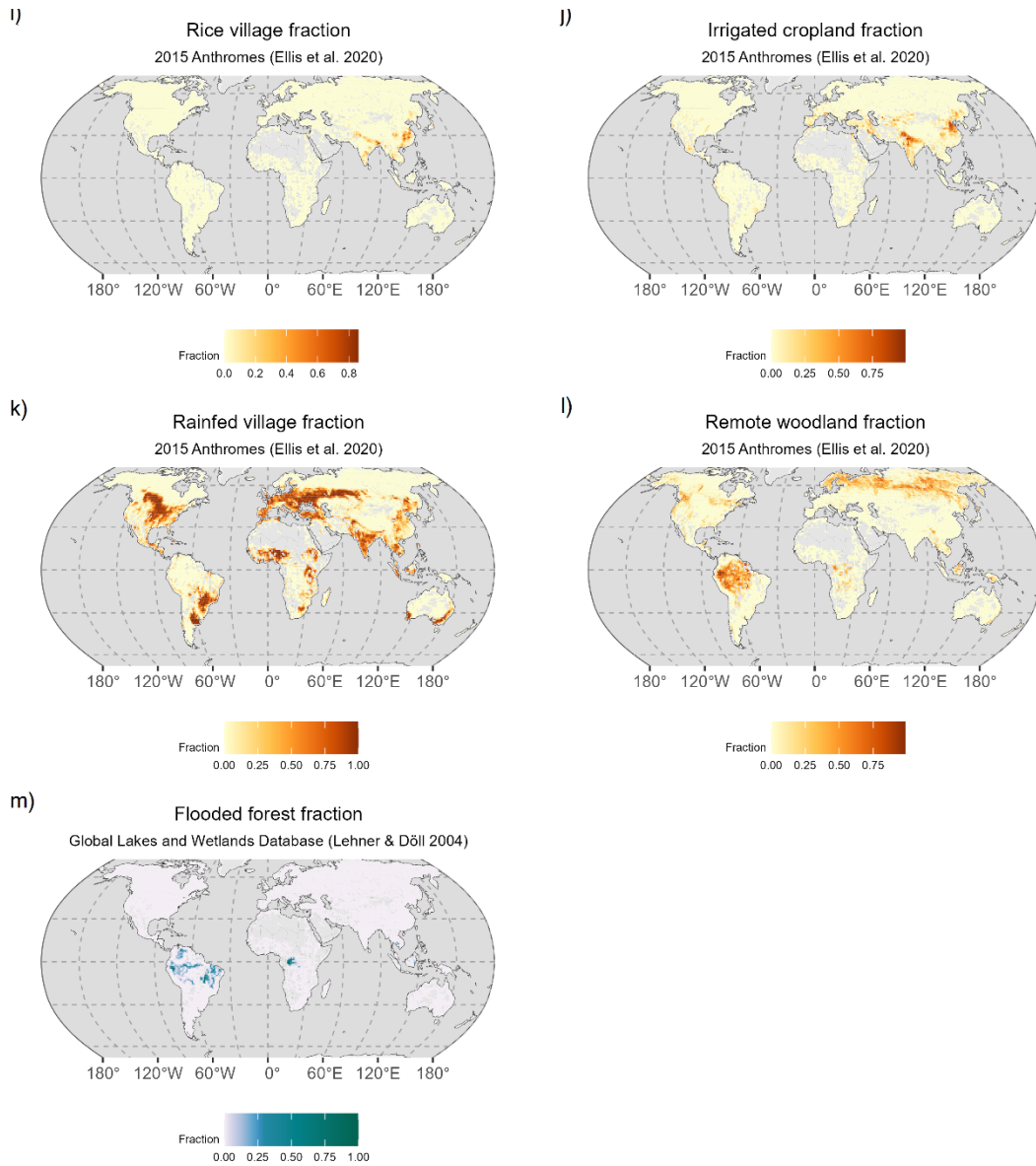


Figure S1 (cont.). Geographical distribution of the thirteen variables for which we analyzed their influence on flooding displacement: (i) Rice fraction; (j) Irrigated cropland fraction; (k) Rainfed fraction; (l) Remote woodland fraction; (m) Flooded forest fraction.

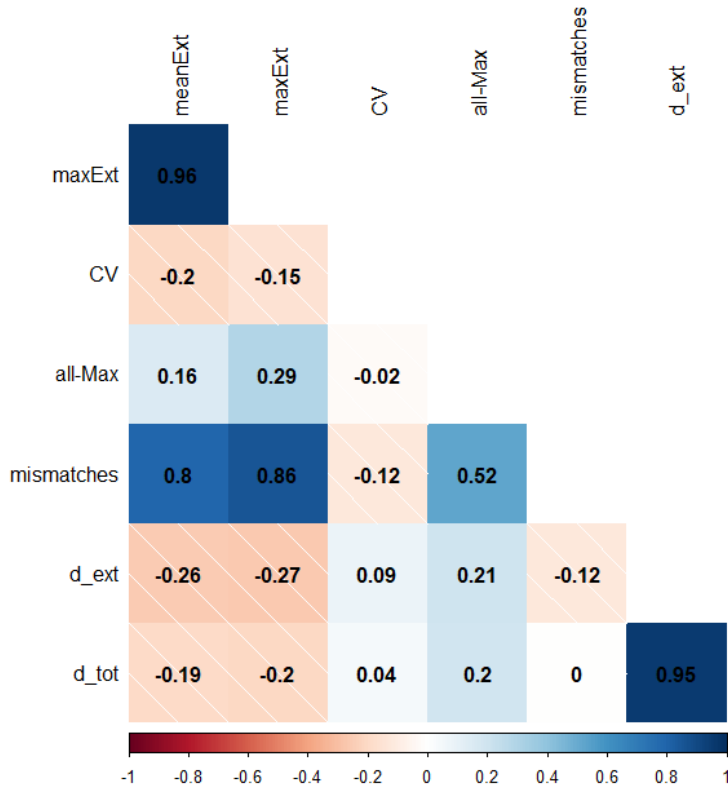


Figure S2. Correlation matrix of typical flooding descriptors and proposed indicators of flooding displacement, all derived from the same dataset (monthly, Landsat-based Global Surface Water; Pekel et al., 2016). Color hue reflects the direction of Spearman’s rho correlation (red = negative; blue = positive), while color intensity reflects the strength of the correlation. maxExt = maximum registered flooded extent per 1-degree grid cell at any month between 1985 and 2020; CV = coefficient of variation (mean / sd); all-Max = absolute difference between the sum of all pixels having been flooded at any point between 1985 and 2020, and the maximum registered flooded event (maxExt); mismatches = absolute differences between the null model of coherent flooding development and the actual, pixel-level flooding frequency distribution; d_ext = extreme displacement index (Eq. 1); d_tot = total displacement index (Eq. 2).

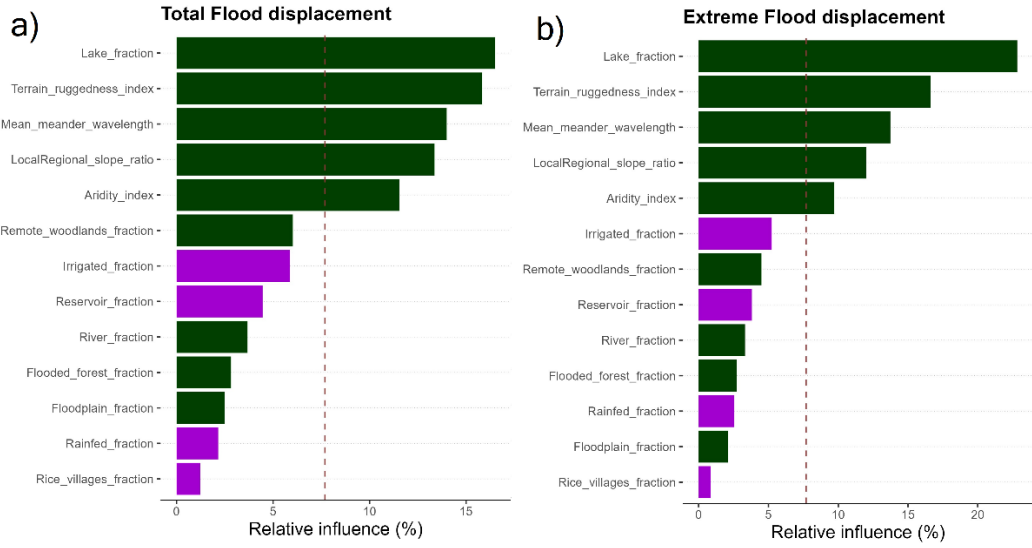


Figure S3. Natural (green) and human (violet) relative influences on (a) total and (b) extreme flooding displacement. Influence values are averaged across a thousand regression tree iterations.

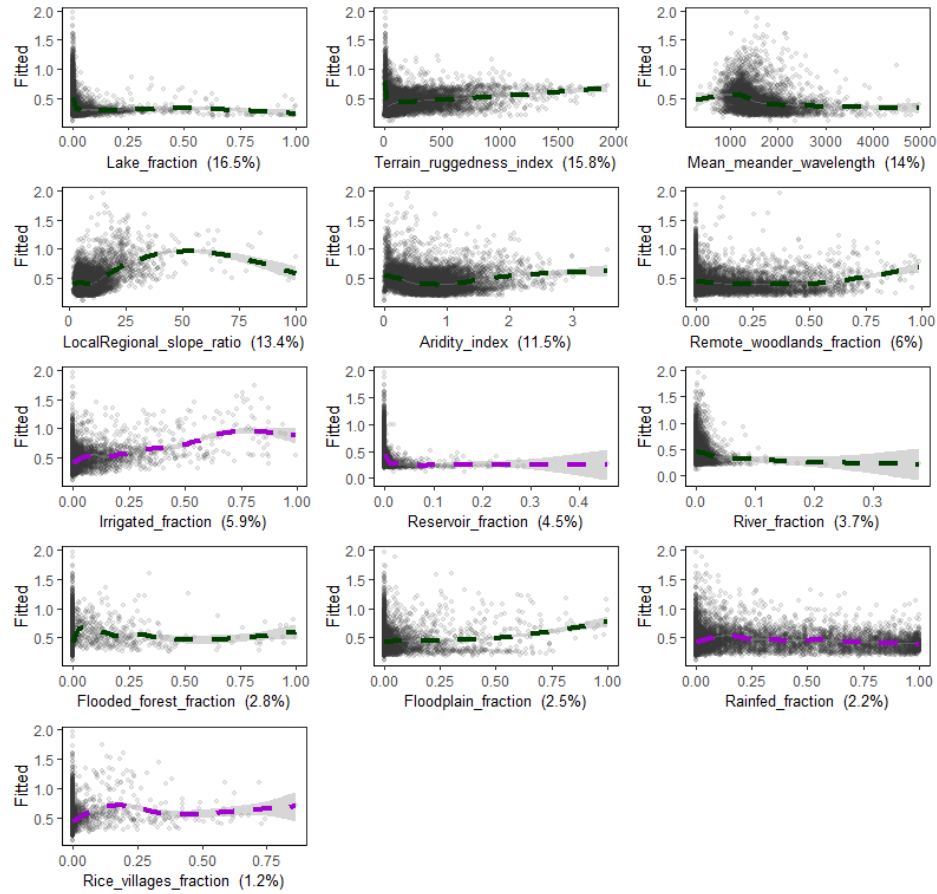


Figure S4. Marginal effect of the natural and induced factors of total flooding displacement (d_{tot}), fitted through general additive models (gam). Values between parenthesis at the x-axis correspond to the relative influence of each variable (averaged across 1000 iterations).

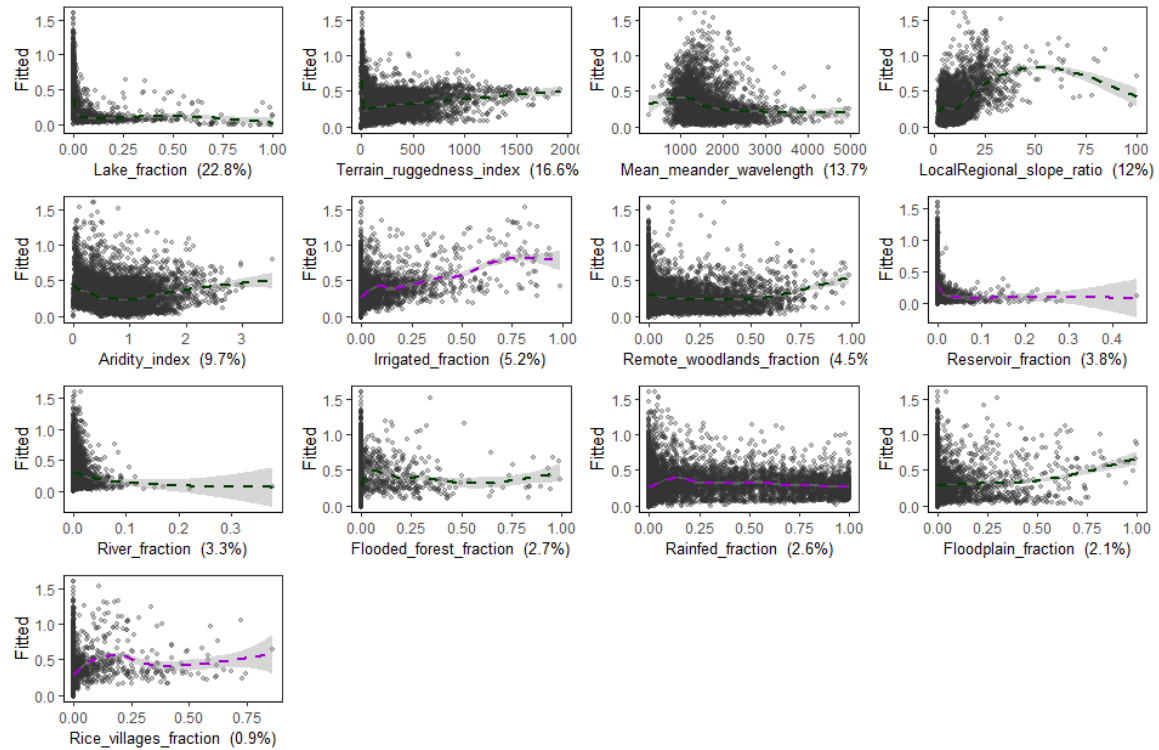


Figure S5. Marginal effect of the natural and induced factors of extreme flooding displacement (d_{ext}), fitted through general additive models (gam). Values between parenthesis at the x-axis correspond to the relative influence of each variable (averaged across 1000 iterations).

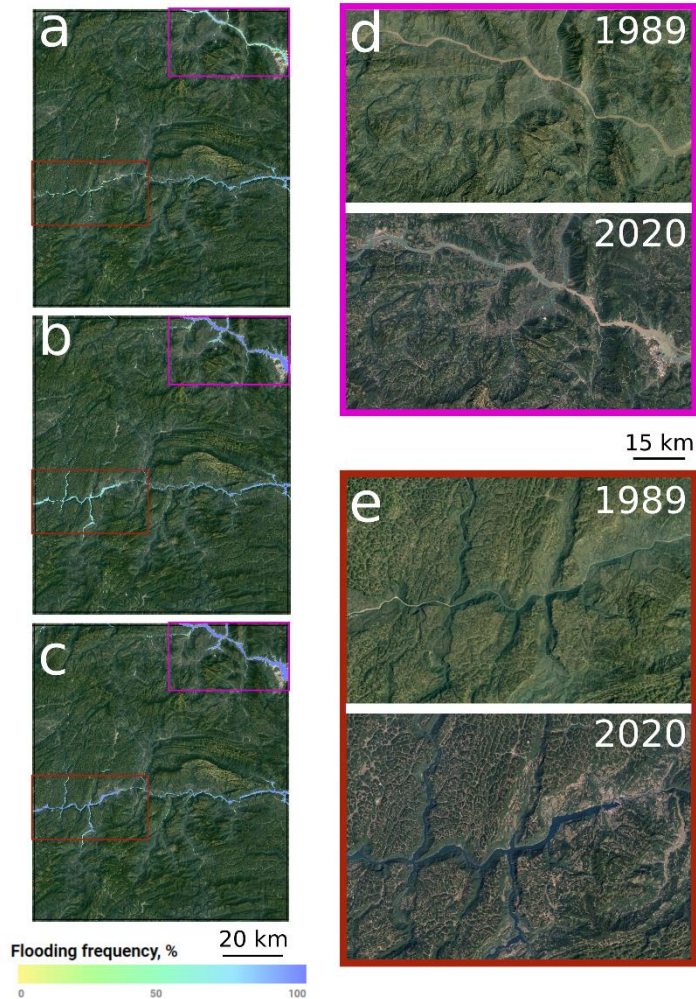


Figure S6. Example of displacement reduction as a result of water reservoir emplacement in a $1^{\circ} \times 1^{\circ}$ landscape centered at 30.5°N , 110.5°E encompassing the Three Gorges Dam (magenta box) and Shuibuiya Dam (red box) which were built and put into operation between 1994 and 2008. (a-c) geographical distribution of flooding frequency for the periods 1985-2002 (i.e., before the operation of either dam); 2003-2021 (i.e., operational period of the TGD but not SD); and 2009-2021 (i.e., operational period of both dams). (d-e) comparative Google Earth images over the Yangtze River and Qingjiang River, respectively, before and after the emplacement of the dams.

References

- Abatzoglou, J. T., Dobrowski, S. Z., Parks, S. A., & Hegewisch, K. C. (2018). *Terraclimate: Monthly climate and climatic water balance for global terrestrial surfaces, university of idaho* [dataset]. Retrieved from https://developers.google.com/earth-engine/datasets/catalog/IDAHO_EPSCOR_TERRACLIMATE doi: 10.1038/sdata.2017.191
- Allen, G. H., & Pavelsky, T. (2018). Global extent of rivers and streams. *Science*, 361 (6402), 585–588. doi: 10.1126/science.aat063
- Elith, J., Leathwick, J. R., & Hastie, T. (2008). *A working guide to boosted regression trees* (Vol. 77) (No. 4). John Wiley & Sons, Ltd. doi: 10.1111/j.1365-2656.2008.01390.x
- Ellis, E., & Klein Goldewijk, K. (2019). *Anthromes 12k full dataset* [dataset]. Retrieved from <https://dataverse.harvard.edu/dataset.xhtml?persistentId=doi:10.7910/DVN/G0QDNQ> doi: 10.7910/DVN/G0QDNQ
- Frasson, R. P. d. M., Pavelsky, T. M., Fonstad, M. A., Durand, M. T., Allen, G. H., Schumann, G., . . . Yang, X. (2019). *Global database of river width, slope, catchment area, meander wavelength, sinuosity, and discharge* [dataset]. Zenodo. Retrieved from <https://doi.org/10.5281/zenodo.2582500> doi: 10.5281/zenodo.2582500
- Lehner, B., & Döll, P. (2004). *Global lakes and wetlands database: Lakes and wetlands grid (level 3)* [dataset]. World Wildlife Fund. Retrieved from <https://www.worldwildlife.org/publications/global-lakes-and-wetlands-database-lakes-and-wetlands-grid-level-3>
- Pekel, J.-F., Cottam, A., Gorelick, N., & Belward, A. S. (2016a). High-resolution mapping of global surface water and its long-term changes. *Nature*, 540 (7633), 418–422. doi: 10.1038/nature2058
- Radinger, J., Alcaraz-Hernández, J. D., & García-Berthou, E. (2018). *Environmental and spatial correlates of hydrologic alteration in a large Mediterranean river catchment*. *Science of The Total Environment*, 639, 1138–1147. doi: 10.1016/J.SCITOTENV.2018.05.227
- Riley, S., DeGloria, S., & Elliot, R. (1999). *A terrain ruggedness that quantifies topographic heterogeneity*. *Intermountain Journal of Science*, 5 (1-4), 23–27